

DAMAGE DETECTION IN CARBON FIBER REINFORCED POLYMERIC
COMPOSITES AND HONEYCOMB SANDWICH PANELS BY ACTIVE
THERMOGRAPHY

by
SEFA KEMAL MANDAL

Submitted to the Graduate School of Engineering and Natural Sciences
in partial fulfillment of
the requirements for the degree of
Master of Science

SABANCI UNIVERSITY
DECEMBER 2019

DAMAGE DETECTION IN CARBON FIBER REINFORCED POLYMERIC
COMPOSITES AND HONEYCOMB SANDWICH PANELS BY ACTIVE
THERMOGRAPHY

APPROVED BY:


Prof. Dr. Mehmet Yıldız
(Thesis Supervisor)


.....

Assoc. Prof. Dr. Burcu Saner Okan


.....

Asst. Prof. Dr. Fatih Ertuğrul Öz


.....

DATE OF APPROVAL: 09.12.2019

© Sefa Kemal Mandal 2019

All Rights Reserved

ABSTRACT

DAMAGE DETECTION IN CARBON FIBER REINFORCED POLYMERIC COMPOSITES AND HONEYCOMB SANDWICH PANELS BY ACTIVE THERMOGRAPHY

SEFA KEMAL MANDAL

Manufacturing Engineering M.Sc. Thesis, December 2019

Thesis Supervisor: Prof. Mehmet Yıldız

Keywords: Carbon Fiber Reinforced Polymeric Composites, Sandwich Structures, Phenolic Resin, Non-destructive Testing, Lock-in Thermography, Pulse Thermography, Acoustic Emission

Infrared thermography is one of the effective non-destructive testing methods for damage characterization and identification in structural materials. Infrared thermography induces a temperature variation on the specimen and monitors the surface temperature to detect defects deep inside the structure. It offers advantages such as being a non-contact inspect method, the capability to scan large surface area and recording in real-time. Although various techniques have been developed for infrared thermography, lock-in thermography (LT) and pulse thermography (PT) are the most preferred ones due to their rapid detection and in-service applicability. LT method uses sinusoidal heat waves in different frequencies, whereas PT, employs an instantaneous heat pulse to increase the specimen's temperature and monitor its evolution to identify the defects due to manufacturing and service conditions.

This thesis focuses on both lock-in and pulse active thermography methods are used to detect different types of defects to assess the feasibility of these methods for non-

destructive testing. To achieve this goal, delamination was first created in carbon fiber reinforced polymeric composites (CFRPC) during manufacturing, and then examined and compared by two methods. Secondly, delamination, liquid ingress and debonding were created artificially during/after manufacturing in a glass/phenolic prepreg with NomexTM honeycomb core sandwich composites which is a widely used material in the aviation industry. The results were presented comparatively on the basis of advantages and disadvantages. Moreover, the results were examined with acoustic emission (AE) method to have a better understanding of the delaminated sandwich structure.

Finally, it is concluded that the most appropriate thermography method is LT method as compared to another method, i.e. PT, used in the study in terms of depth and characterization of the defect. Using the results obtained in this thesis, barely visible damage modes in CFRPC and phenolic-based sandwich structures used in the aviation industry were detected by active thermography. In addition, the damage modes that occurred during the bending tests were correlated with AE. This makes a great contribution to the improvement of structural health monitoring of these materials in the field of the aerospace industry.

ÖZET

KARBON ELYAF TAKVİYELİ POLİMERİK KOMPOZİTLER VE BALPETEĞİ SANDVIÇ PANELLERDE AKTİF TERMOGRAFI YÖNTEMİ İLE HASAR TESPİTİ

SEFA KEMAL MANDAL

Üretim Mühendisliği, Yüksek Lisans Tezi, Aralık 2019

Tez Danışmanı: Prof. Dr. Mehmet Yıldız

Anahtar Kelimeler: Karbon Elyaf Takviyeli Polimerik Kompozitler, Sandviç Yapılar, Fenolik Reçine, Tahribatsız Hasar Analiz Testi, Kilitli Termografi, Flaş Termografi, Akustik Emisyon

Kızılötesi termografi, yapısal malzemelerde hasar karakterizasyonu ve tanımlanması için etkili bir tahribatsız muayene yöntemlerinden biridir. Bu yöntem, numunede bir sıcaklık değişimini tetikler ve yapının derinliklerindeki hataları tespit etmek için yüzey sıcaklığını izlenmesini sağlar. Temassız kontrol yöntemi olan kızılötesi termografi yöntemi, geniş yüzey alanını tarama ve gerçek zamanlı kayıt yapma gibi avantajları da sunar. Kızılötesi termografi için çeşitli teknikler geliştirilmiş olmasına rağmen, kilitli termografi (LT) tekniği ile flaş termografi (PT) tekniği hızlı tespiti ve servis kullanımı sırasında uygulanabilirliği gibi nedenlerinden dolayı tahribatsız hasar yöntemlerinden en çok tercih edilenlerdir. LT tekniği, farklı frekanslarda sinüzoidal bir ısı dalgası kullanır. Buna karşın PT yöntemi ise, numune sıcaklığını uyarmak için anlık bir ısı darbesi sağlar ve hataları tanımlamak için numune sıcaklığının evrimini izler.

Bu tez, hem LT hem de PT yöntemlerine odaklanmaktadır ve bu yöntemlerin tahribatsız testler için uygulanabilirliğini değerlendirmek üzere farklı türdeki kusurları tespit etmek için kullanılmaktadır. Bu amaca ulaşmak için, ilk önce üretim sırasında karbon fiber takviyeli polimerlerde (CFRP) delaminasyon oluşturuldu ve daha sonra iki yöntemle

incelendi ve karşılaştırıldı. İkincisi, havacılık endüstrisinde yaygın olarak kullanılan bir malzeme olan Nomex™ balpeteği çekirdekli sandviç kompozitlerle bir cam / fenolik prepreglerde üretim sırasında / sonrasında yapay olarak delaminasyon, sıvı girişi ve bağ ayrışması oluşturuldu. Sonuçlar, avantaj ve dezavantajlar temelinde karşılaştırmalı olarak sunulmuştur. Ayrıca, delamine olmuş sandviç yapıyı daha iyi anlayabilmek için sonuçlar akustik emisyon (AE) yöntemiyle incelenmiştir.

Bu çalışmanın sonuçlandırılmasıyla, kusurun derinliği ve karakterizasyonu açısından çalışmada kullanılan diğer yöntemlere kıyasla en uygun yöntemin LT yöntemi olduğu söylenebilir. Bu tezde elde edilen sonuçlar sayesinde, havacılık endüstrisinde kullanılan, el ve çıplak gözle tespit edilemeyen CFRP ve fenolik bazlı sandviç yapılarda hasar modları aktif termografi ile tespit edilmiştir. Ek olarak, bükme testleri sırasında meydana gelen hasar modları AE ile doğrulanmıştır. Bu çalışma, havacılık alanında katastrofik bir arızayı önlemek için bu malzemelerin geliştirilmesine büyük katkı sağlamaktadır.

To my beloved great family...

ACKNOWLEDGEMENTS

I personally want to extend my most special and sincere thanks to my thesis supervisor Prof. Dr. Mehmet Yıldız for his guidance, encouragement, supportive and constructive attitude throughout my master's degree. I am proud to be one of his students.

I would also like to thank Assoc. Prof. Burcu Saner Okan and Asst. Prof. Fatih Ertuğrul Öz for their valuable time and their supportive and constructive feedback on this thesis.

My profound thanks go to Dr. Jamal Seyyed Monfared Zanjani, M.Sc. Yiğit Özcan, M.Sc. Murat Tansan, Kerem Dörtkaşlı, M.Sc. Isa Emami Tabrizi, M.Sc. Ragıp Orkun Seçer, M.Sc. Faruk Sapmaz, and M.Sc. Bora Gönül. I am lucky that they helped me every time I requested during my research. Without their support and assistance, most of this study would not have arisen.

I would like to thank Ertan Acar, Cuma Koşar, Nuray Tatlı, Serap Aslan, Sinan Karasu, Mehmet Olcaz, Burak Yurt, Sezgin Şahin, Kadir Erdoğan for their help and support in Sabanci University Integrated Manufacturing Research and Application Center.

I would like to express my sincere thanks to my close friends, Erinç Güney Gül, Çağrı Özeçoğlu, Hakan Özlen, Çağlayan Çetin, Fatih Uslu, Emincan Bilgeç, Melih Özen, Selim Arık and Fatih Elbir for being motivated and happy for me in most of my life.

Finally, I would like to extend my deepest sincere to Ayşe Erbey, my great family, Süleyman Yaman and of course Oddish and Hera for their unrequited love and encouragement throughout my whole life journey. Especially to my mother who being with me and helping me all my life.

This study has been supported by Sabanci University Faculty of Engineering and Natural Sciences Dean's Office, Sabanci University – Integrated Manufacturing Technologies Research and Application Center. The authors would like to acknowledge the material supply support provided by KordSA Composite Business Unit in KordSA Composite Technologies Center of Excellence.

TABLE OF CONTENTS

ABSTRACT.....	i
ÖZET	iii
ACKNOWLEDGEMENTS	vi
TABLE OF CONTENTS	vii
LIST OF FIGURES	ix
LIST OF TABLES	xi
LIST OF ABBREVIATIONS	xii
Chapter 1 INTRODUCTION	1
1.1. Outline of the thesis	1
1.2. Literature Review	2
1.2.1. Carbon Fiber Reinforced Polymeric Composites	2
1.2.2. Honeycomb Sandwich Structures	2
1.2.3. Non-destructive Testing.....	3
1.2.3.1. Infrared Thermography	5
1.2.3.1.1. Lock-in Thermography	5
1.2.3.1.2. Pulse Thermography	6
1.2.3.2. Acoustic Emission	7
Chapter 2	9
Non-destructive Testing of CFRPC by Active Thermography	9
2.1. Experimental	9
2.1.1. CFRPC Materials and Manufacturing	9
2.1.1.1. First CFRPC Sample.....	9
2.1.1.2. Second CFRPC Sample	10
2.1.1.3. Third Sample.....	11
2.2. Thermography Experimental Setup	12
2.2.1. LT and PT Test Measurements	12
2.3. Results and Discussions	13
2.3.1. First sample.....	13

2.3.2. Second Sample.....	14
2.3.2.1. LT and PT results.....	14
2.3.3. Third Sample.....	16
Chapter 3	18
Non-destructive testing of sandwich structures by active thermography verified with AE	18
3.1. Experimental	18
3.1.1. Phenolic resin/GF/Honeycomb Composite Materials and Manufacturing...	18
3.1.1.1. First Phenolic Resin Sandwich Sample	19
3.1.1.2. Second Phenolic Resin Sandwich Sample.....	20
3.1.1.3. Third Phenolic Resin Sandwich Sample.....	20
3.2. Experimental Setup for Phenolic Resin Sandwich Samples	21
3.2.1. Thermography Test Setups	21
3.2.2. AE Test Setup	23
3.3. Results and Discussion.....	24
3.3.1. Inspection of Liquid Ingress by LT and PT	24
3.3.2. Inspection of Debonding by LT and PT	26
3.3.3. Inspection of Delamination by LT and PT	29
3.3.4. Comparison of AE with LT	30
Chapter 4 CONCLUSIONS.....	38
REFERENCES.....	40

LIST OF FIGURES

Figure 1.1 Distribution of used materials in Boeing 787 [4]	2
Figure 1.2 Representation of aircraft interior [7], [8]	3
Figure 1.3 Representation of cabin interior of aircraft [7], [8]	3
Figure 1.4 Defect types in sandwich composite plate [23]	4
Figure 2.1 Drawing of two-hole defects sample	10
Figure 2.2 Drawing of six-hole defects sample	10
Figure 2.3 Representation of (a) hot press and (b) CF sandwich sample	11
Figure 2.4 (a) Instron 5982 electro-mechanical test machine, (b) Damaged surface of CF sandwich structure	12
Figure 2.5 LT test setup (left image) (a) represents halogen lamps, (b) represents IRT Camera, PT test setup (right image) (c) represents CF sample and (d) represents flash lamp	13
Figure 2.6 LT results of the two-hole defects (first sample) with different frequencies (a) 0.01 Hz, (b) 0.02 Hz, (c) 0.03 Hz, (d) 0.04 Hz, (e) 0.08 Hz, (f) 0.07 Hz	14
Figure 2.9 LT results of six-hole defects (second sample) with different frequencies (a) 0.01 Hz, (b) 0.02 Hz, (c) 0.01 Hz with different region of interest, (d) 0.05 Hz....	15
Figure 2.10 PT results of six-hole defects (second sample) (a) 1 Hz flash frequency, (b) 1 Hz flash frequency with different region of interest.....	16
Figure 2.11 LT results of CF sandwich plate after compression test (a) at 0.1 Hz LT frequency focusing 15000 N defect, (b) at 0.1 Hz LT frequency focusing 3000 N defect.....	17
Figure 2.12 PT results of CF sandwich plate after compression test (a) 1 Hz frequency focusing 15000N defect, (b) 5 Hz frequency with different ROI.....	17
Figure 3.1 Arrangement of sandwich panels during fabrication	19
Figure 3.2 Representative illustration of embedding paraffin oil in cells before curing	19
Figure 3.3 A representative illustration of embedding Teflon film into sample to create debonding.....	20
Figure 3.4 Representation of delamination formation	21
Figure 3.5 LT test set-up for the examination of phenolic sandwich structures.....	22
Figure 3.6 PT test set-up for the examination of phenolic sandwich structures	22
Figure 3.7 Detection depth & thermal diffusion length (mm) vs. modulated frequency	23
Figure 3.8 Placing AE sensors during 3-point test	24

Figure 3.9 Raw image of LT for liquid ingress test in sandwich composite	24
Figure 3.10 LT images: (a) at frequency of 0.01 Hz and (b) at frequency of 0.05 Hz for liquid ingress test in sandwich composite.....	25
Figure 3.11 PT images: (a) raw image and (b) at frequency of 1 Hz for liquid ingress test in sandwich composite.....	25
Figure 3.12 Raw image of LT for debonding in sandwich composite	27
Figure 3.13 LT images: (a) at frequency of 0.01 Hz and (b) at frequency of 0.07 Hz for debonding in sandwich composite.....	27
Figure 3.14 Raw image of PT for debonding in sandwich composite.....	28
Figure 3.15 PT images: (a) at frequency of 1 Hz (phase mode) and (b) at frequency of 1 Hz (amplitude mode) for debonding in sandwich composite.	28
Figure 3.16 LT images: (a) raw image, (b) at frequency of 0.01 Hz, c) at frequency of 0.002 Hz for 3-point bending test in sandwich composite captured from non-defective side	29
Figure 3.17 PT images: (a) raw image, (b) at frequency of 1 Hz for 3-point bending test in sandwich composite captured from non-defective side.....	29
Figure 3.18 Test interruption levels of specimens with respect to Load vs. Displacement diagram	31
Figure 3.19 The LT results of reference sample (untested): (a) FT at front image frequency of 0.002 Hz (phase rain mode), (b) front image frequency of 0.002 Hz (real/imag iron mode)	34
Figure 3.20 AE and LT results of Sample 1: (a) cumulative AE energy, (b) average amplitude values of AE, (c) front image frequency of 0.01 Hz (phase rain mode), (d) front image frequency of 0.01 Hz (amplitude rain mode), (e) front image frequency of 0.01 Hz (real/imag rain mode), (f) front image frequency of 0.01 Hz (imag default mode)	35
Figure 3.21 AE and LT results of Sample 2 (a) cumulative AE energy, (b) average amplitude values of AE, (c) front image frequency of 0.002 Hz (phase iron mode), (d) rear image frequency of 0.002 Hz (real/imag rain mode), (e) rear image frequency of 0.002 Hz (real/image).....	36
Figure 3.22 AE and LT results of Sample 3: (a) cumulative AE energy, (b) average amplitude values of AE, (c) front image frequency of 0.002 Hz (phase rain mode), (d) front image frequency of 0.002 Hz (phase iron mode), (e) rear image frequency of 0.002 Hz (real/imag rain mode).....	37

LIST OF TABLES

Table 1-1 Common defect types in honeycomb sandwich structures	4
Table 3-1 Estimated depth of defect at given frequency	23

LIST OF ABBREVIATIONS

AE: Acoustic Emission
ASTM: American Society for Testing and Materials
CF: Carbon Fiber
CFRPC: Carbon Fiber Reinforced Polymeric Composites
cm: Centimeter
D: Diameter
EC: Eddy Current
F: Force
FEM: Finite Element Method
FT: Fourier Transform
FFT: Fast Fourier Transform
GF: Glass fiber
GFRP: Glass Fiber Reinforced Polymer
Hz: Hertz
IR: Infrared Radiation
J: Joule
kN: kilo-newton
LT: Lock-in Thermography
ms: millisecond
mK: millikelvin
N: Newton
NDT: Non-destructive Testing
NDE: Non-destructive evaluation
PT: Pulse Thermography
PPT: Pulsed Phase Thermography
QI: Quasi-isotropic
r: radius
ROI: Region of Interest
RT: Radiography Testing
ST: Shearography Testing
t: time

UT: Ultrasonic Testing

VT: Vibrothermography

XCT: X-ray Computed Tomography

XP: Cross-ply

Chapter 1

INTRODUCTION

1.1. Outline of the thesis

Chapter 1 covers the literature review in relation to carbon fiber reinforced polymeric composites (CFRPC), sandwich structures and non-destructive testing (NDT) methods used in this thesis.

Chapter 2 of this thesis covers the manufacturing steps of the CFRPC, the artificial defects given during manufacturing and the examination of these defects after manufacturing by two thermography methods.

Chapter 3 includes the examination of three artificial defects created during and after the fabrication of glass fiber reinforced phenolic resin by LT and PT separately. The damage detectability of these two active thermography methods for three different defects was compared. In addition to Chapter 3, out-of-plane bending tests were performed with simultaneous acoustic emission (AE) registration. Tests were interrupted at different load levels and then registered AE events compared with captured LT images.

This study concludes in Chapter 4 on the basis of results obtained in Chapter 2 and Chapter 3.

1.2. Literature Review

1.2.1. Carbon Fiber Reinforced Polymeric Composites

The use of carbon fiber reinforced polymers has increased considerably in recent years especially in the aerospace, automotive and marine industry due to their advanced specific properties such as high strength-to-weight ratio, corrosion resistance, improved fatigue behavior, high chemical and environmental resistance, high impact strength, etc. [1]–[3]. For example, as seen in Figure 1.1 about 50% of all materials used in a commercial Boeing 787 are made of composite materials which shows their importance in the aerospace industry [4].

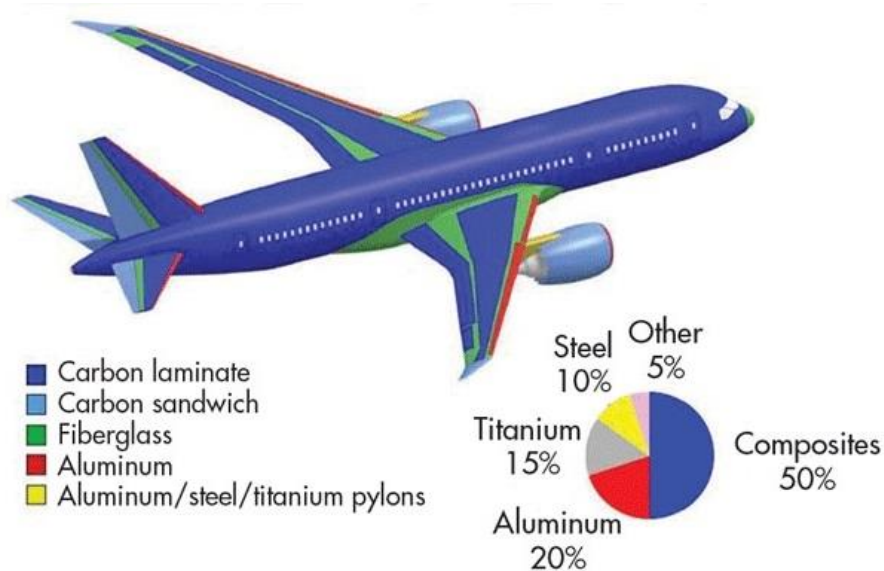


Figure 1.1 Distribution of used materials in Boeing 787 [4]

1.2.2. Honeycomb Sandwich Structures

In recent years, the application of honeycomb sandwich composites has increased considerably in aerospace, automotive and marine industries due to their splendid out-of-plane compressive and shear strengths, process flexibility, lightweight, and high chemical and heat resistance. However, this group of structural materials is sensitive to failure and damage under static and impact loadings or environmental causes such as fluid ingress [1], [5], [6]. In addition, honeycomb sandwich materials, especially phenolic resin honeycomb sandwich materials, are often used in the cabin interior of aircraft besides

using CF sandwich materials in the exterior of the aircraft. Sandwich structures used in the cabin interior are shown in Figure 1.2 and Figure 1.3.



Figure 1.2 Representation of aircraft interior [7], [8]



Figure 1.3 Representation of cabin interior of aircraft [7], [8]

1.2.3. Non-destructive Testing

Structural health monitoring approaches together with non-destructive testing (NDT) methods are emerging as is essential damage assessment and safety control methodology in composite materials in many advanced applications such as aerospace. Periodic damage analyzes and safety controls using non-destructive testing or evaluation (NDT&E) is required for identification and evaluation of possible damage in the

engineering structure without causing any harm or damage to their design and integrity [1], [9]–[11]. Some of the typical defect types that are detected using NDT&E methods are illustrated in Figure 1.4. There are variety of NDT methods for damage detection such as X-ray computed tomography (XCT) [12] [13], ultrasonic testing (UT) [14], shearography testing (ST) [15], [16], pulsed phase thermography (PPT) [17], [18], vibrothermography (VT) [19], radiography testing (RT) [20], eddy current (EC) [21], [22]. However, most of the aforementioned NDT methods have limitations such as being time-consuming, labor-intensive and having limited accuracy. In this regard, infrared thermography and acoustic emission (AE) methods are one of the most effective damage detection methods which are capable of determining the initiation and propagation of damage and identify the failure mode. The description of general defect types in composite sandwich structures is demonstrated in Table 1-1.

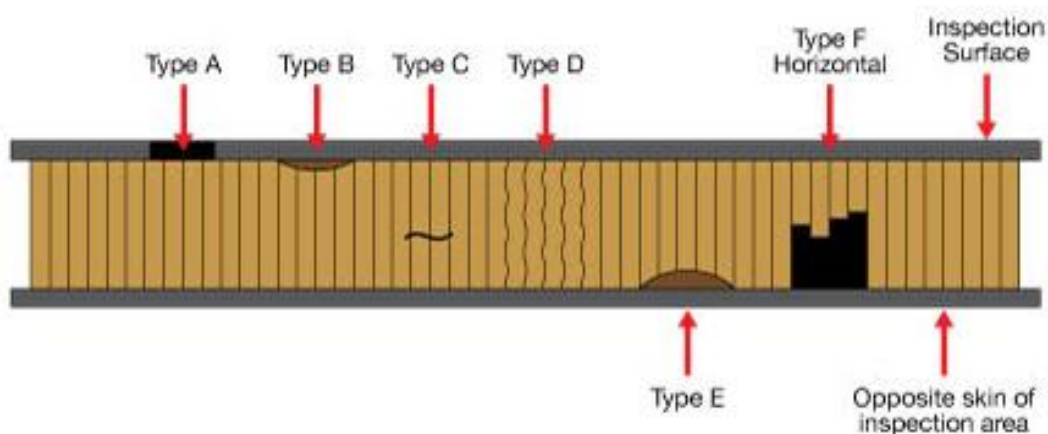


Figure 1.4 Defect types in sandwich composite plate [23]

Type A	Delamination
Type B	Debonding outer skin
Type C	Crack initiate
Type D	Crushed core
Type E	Debonding inner skin
Type F	Liquid ingress

Table 1-1 Common defect types in honeycomb sandwich structures

1.2.3.1. Infrared Thermography

Infrared thermography (IRT) is one of the most prominent NDT methods for sandwich structures. IRT uses thermal perturbation to identify the defects on the surface or bulk of a structure by monitoring the temperature variation on the specimen surface. Any discontinuities in the surface or bulk of the structure change the heat propagation pattern inside the structure which will be reflected in the surface temperature [24]–[26].

There are several studies in which IR Thermography, especially LT and PT, is used for the detection and identification of damage mode in composite materials. For example, Ishikawa et al. [27] used a CO₂ laser scanning device as a heat source for NDE of carbon fiber reinforced plastic. This study demonstrates that there is no big difference between laser scanning source and flash lamp heat source in terms of phase and temperature behavior after heating. According to numerical and experimental results, the temperature contrast on the defective surface varies according to the scanning direction. Also, they showed that defects in the sample were detected using a laser heat source at a distance of 10 meters [27]. Swiderski [28] used IRT (LT and PT methods) with laser thermal stimulation to predict defect in CF based multilayer composites through numerical and experimental tests. According to the results, enhancement of probability of detecting defects deeper in the sample is related to increasing laser beam intensity, however, this situation creates the risk of permanent damage to the sample. Nevertheless, the results state that using a laser beam as a heat source is possible in the field of IRT of CF-based multilayer composites [28]. Ibarra-Castanedo et al. [29] created delamination, excessive adhesive and core crush in honeycomb sandwich material in order to compare LT, PT and VT methods. According to results, they concluded that three IRT approaches could be useful to detect damages in honeycomb structures.

1.2.3.1.1. Lock-in Thermography

Lock-in thermography (LT) is one of the most commonly used IRT methods lending its popularity to its rapid detection procedure, in-service applicability, portable equipment and being a non-contact technique. In this method, the temperature variation on the surface of the material is attained during the propagation and adsorption of a modulated heat through it. The reflection of the modulated thermal wave by defects results in a transformation on the response wave amplitude and phase [24], [25], [30], [31]. Detailed analysis of the temperature-time history by applying Fourier Transform (FT) based image

processing methods on each pixel provides an insight into the defect state of the structure, in other words, since defects act as a thermal barrier during heat propagation and consequently they vary the phase and amplitude at defected areas as compared to sound regions of material. From the one-dimensional solution of Fourier's Law for a sinusoidal thermal wave transmission from a semi-infinite homogeneous material, the thermal diffusion length is given as follows [32]:

$$\mu = \sqrt{\frac{2\alpha}{\omega}} = \sqrt{\frac{\alpha}{\pi f}} \quad (1)$$

where ω is modulation frequency ($\omega = 2\pi f$ and f is the wave frequency in Hz and α is thermal diffusivity), and thermal diffusion length is a function of thermal diffusivity, α , and wave frequency, f . The thermal diffusivity of material is given by:

$$\alpha = \frac{\kappa}{\rho c_p} \quad (2)$$

where κ is the thermal conductivity, ρ is the density and c_p is specific heat (at constant pressure) of material.

The depth of the defect z can be determined by using the thermal diffusion length formula:

$$z = r_l \mu \quad (3)$$

where r_l is correlation constant, and r_l values range from 1.5 to 2 [33].

1.2.3.1.2. Pulse Thermography

Pulse thermography method uses a short pulse of energy in the form of flash-light to disturb the thermal equilibrium of the structure. The heat generated by the pulsed energy propagates from the surface of the structure towards the subsurface. The presence of any defect on the surface or bulk of the structure returns the pulsed heat to the specimen surface. Therefore, a localized high-temperature zone will be observed in the damaged area which can be used to determine the location, intensity and depths of the defects.

Temperature field, $T(x,t)$, in PT is the result of solving 1D thermal diffusion equation which is given by:

$$\frac{\partial^2 T}{\partial x^2} = \frac{1}{\alpha} \frac{\partial T}{\partial t} \quad (4)$$

where T is the temperature and α is thermal diffusivity of the material. Since an ideal heat flux is defined as a pulse with a very short duration of intense unit-area, one-dimensional Fourier equation for the propagation of a Dirac delta function as the basis of PT method is given by [34]:

$$T(x, t) = T_0 + \frac{Q}{e\sqrt{\pi t}} \exp\left(\frac{-x^2}{4\alpha t}\right) \quad (5)$$

where e is the thermal effusivity ($e = \sqrt{k\rho c}$), Q is the quantity energy absorbed by the surface, T_0 is initial temperature, t is the time, and x is the depth of the material. At the surface, $x = 0$, Equation 5 reduces to:

$$T(0, t) = T_0 + \frac{Q}{e\sqrt{\pi t}} \quad (6)$$

Equation 6 tells us that temperature on the surface decreases approximately with time and relates the heat penetration coefficient which is the rate of heat absorbance by the material.

1.2.3.2. Acoustic Emission

Acoustic Emission (AE) is one of the most effective damage detection methods which can detect the initiation and propagation of damage and enables identifying the failure modes inside material through clustering methods. AE is especially crucial to detect damage in visually inaccessible regions, such as matrix cracks in the inner plies of a polymer matrix laminates structure. The determination of the damage types by using AE is as follows; after applying the clustering procedure, stress-strain curves are combined

with cumulative energy release of registered acoustic emission hits. This energy is obtained by dividing the integral of the voltage signal by the reference resistance on the package of AE waveform.

There are few studies in which the AE technique is used for damage mode identification in composite materials [10], [35]–[43]. For example, Tabrizi et al. [41] applied AE registration to glass/carbon fiber reinforced hybrid composites under bending and tensile loads. Afterward, they could distinguish damage types through the K-mean algorithm. Moreover, they verified the results with a simulation of the experimental tests by means of finite element method based on refining zigzag theory [41]. Uzal et al. [44] used a progressive damage analysis method based on finite element method (FEM) to predict progressive failure modes in GFRP skinned sandwich structures containing egg crate core. AE method was applied during tension tests of quasi-isotropic (QI) and cross-ply (XP) laminates, to determine the first ply failure levels. Then the unidirectional material properties of the composite material were back-calculated from the determined first ply failure level. These properties were used in FEM which built a consistent relationship between the AE results and predicted failure modes [44].

Chapter 2

In this chapter, various CFRPC samples have been manufactured in different orientations and layers to measure the defect detectability of the LT and PT methods. Some samples were given artificial defects during manufacturing. In addition, impact tests were applied to the produced carbon fiber samples and damage analyses were performed with LT and PT. Moreover, a carbon fiber sandwich plate was manufactured to evaluate the surface imperfections after the compression test.

Non-destructive Testing of CFRPC by Active Thermography

2.1. Experimental

2.1.1. CFRPC Materials and Manufacturing

In order to evaluate the detectability of LT and PT methods, various types of defected samples were fabricated.

2.1.1.1. First CFRPC Sample

The first CFRPC sample was made of carbon fiber prepreg sample manufacturing with cross-ply laminates. The sample has 12 layers and has dimensions of 30 cm by 30 cm. Also, it has two-hole defects which given during manufacturing artificially with a radius of 5 cm, and the first hole defect of these is on the third layer of the specimen, the second one is on the sixth layer of the specimen. Hole defects and the two-dimensional drawing of the sample are given in Figure 2.1.

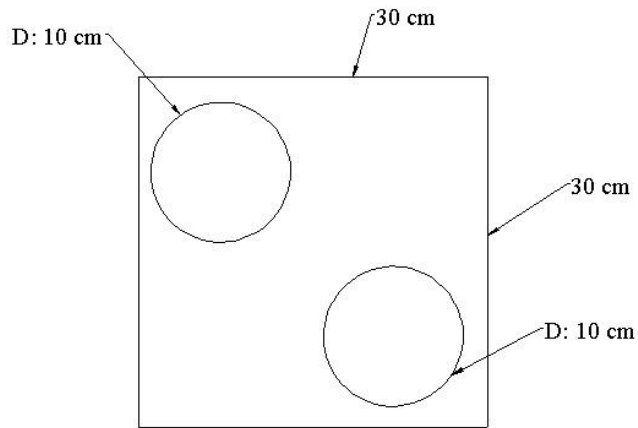


Figure 2.1 Drawing of two-hole defects sample

2.1.1.2. Second CFRPC Sample

The second CFRPC sample was made of carbon fiber prepreg sample manufacturing with cross-ply laminates. The sample has 12 layers and has dimensions of 30 cm by 30 cm. Yet, in this instance, the size of the hole-defects has been altered and the number of defects has been increased. It has six-hole defects with a radius of 5 cm, 2.5 cm, 2 cm, 1.5 cm, 1 cm, and 0.5 cm, respectively. Hole defects and the two-dimensional drawing of the sample are given in Figure 2.2.

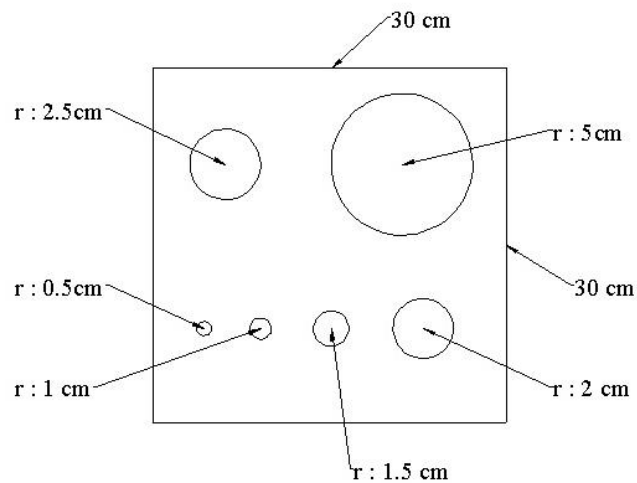


Figure 2.2 Drawing of six-hole defects sample

2.1.1.3. Third Sample

In order to inspect the sample with thermography, the specimen was prepared in a different orientation (0/90/0/90 | 90/0/90/0) and it was cured at 120°C for one hour with 5 tones hot press. Manufacturing processes and the sample can be seen in Figure 2.3-(a) and Figure 2.3-(b).



Figure 2.3 Representation of (a) hot press and (b) CF sandwich sample

After the manufacturing of the CF honeycomb sandwich panel, the sample was subjected to compression tests in order to perform damage detection with the infrared thermography. The loads were applied to the sample surface as 3000 N and 15000 N with Instron 5982 electro-mechanical test machine with a capacity of 150 kN. Damaged surface and compression test equipment are given in Figure 2.4 and in Figure 2.4-(a), the upper arrow represents 15000 N and the below arrow represents 3000 N.

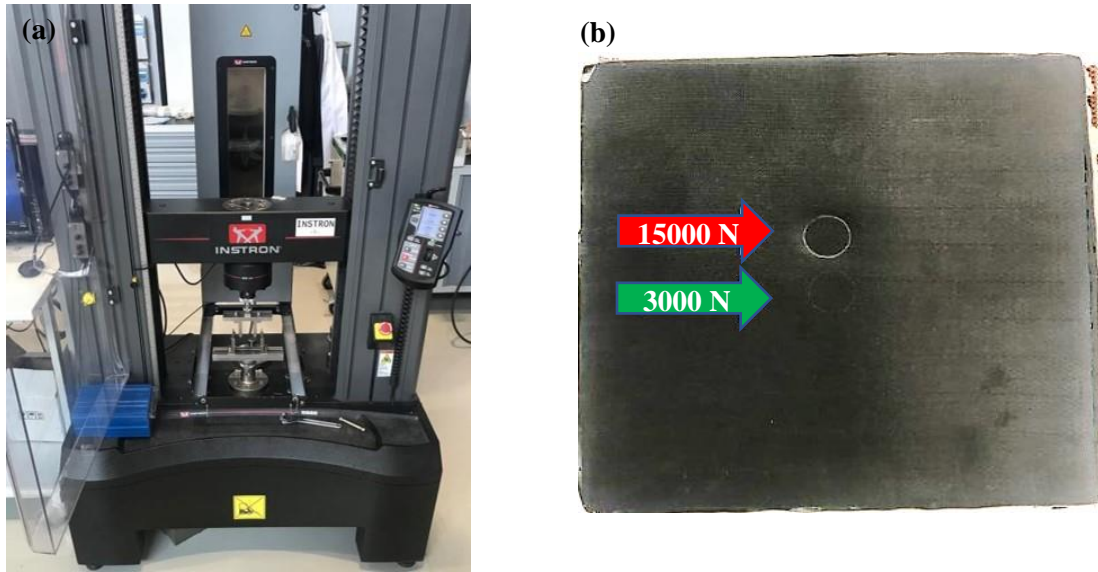


Figure 2.4 (a) Instron 5982 electro-mechanical test machine, (b) Damaged surface of CF sandwich structure

2.2. Thermography Experimental Setup

2.2.1. LT and PT Test Measurements

The LT and PT experiments were performed by using three Xenon halogen lamps (for LT) and flash lamps (for PT) as a heat source, a computer and FLIR X6580 SC with 25mm optical lens thermal imaging camera equipped with MWIR 640 x 512 sensor, thermal sensitivity is below 20 mK and has a capability of maximum frame rate at 355 Hz at 640 x 512 pixel. Afterwards, captured images were analyzed by using OTvis 6000 module of DisplayIMG 6 processing software (Edevis GmbH, Stuttgart, Germany) for LT test and by using PTvis 6000 module of DisplayIMG 6 processing software for PT test. Figure 2.5 presents the configuration of thermography tests for LT method (left image) and PT method (right image).

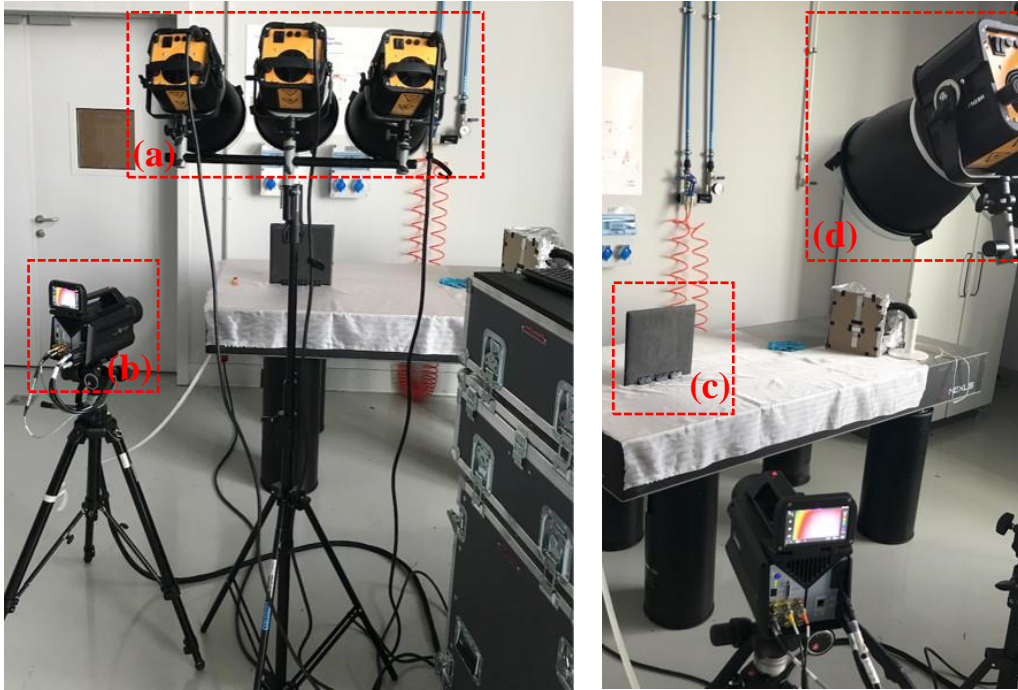


Figure 2.5 LT test setup (left image) (a) represents halogen lamps, (b) represents IRT Camera, PT test setup (right image) (c) represents CF sample and (d) represents flash lamp

2.3. Results and Discussions

2.3.1. First sample

In order to have a clearer and sharper image of the hole-defects in Figure 2.1, different frequencies namely 0.01 Hz, 0.02 Hz, 0.03 Hz, 0.04 Hz, 0.07 Hz and 0.08 Hz were used. The results are phase variation at different parts of the sample for different frequencies are seen in Figure 2.6.

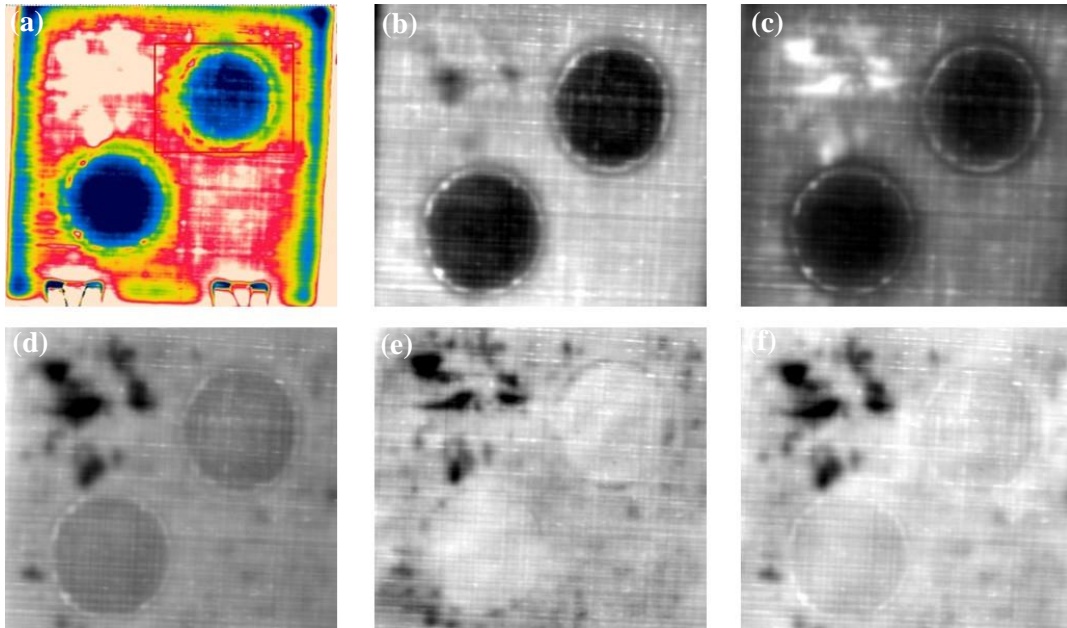


Figure 2.6 LT results of the two-hole defects (first sample) with different frequencies (a) 0.01 Hz, (b) 0.02 Hz, (c) 0.03 Hz, (d) 0.04 Hz, (e) 0.08 Hz, (f) 0.07 Hz

As seen in Figure 2.6, the two hole-defects in the sample are clearly visible when 0.01 Hz and 0.02 Hz are applied. As the value of frequency increases for thermal analysis, the exact size and boundaries of the defects become vague due to a decrease in penetration of thermal waves, this is because thermal diffusion length is directly proportional to the applied frequency which was indicated in Equation 1. However, the overall location of hole defects is identifiable since they are close to the surface of the sample. In conclusion, it can be said that using appropriate frequency for the detection of subsurface defects is crucial in CFRPC.

2.3.2. Second Sample

2.3.2.1. LT and PT results

In order to detect hole-defects in different sizes as depicted in Figure 2.2, different frequencies namely 0.01 Hz, 0.02 Hz and 0.05 Hz were used. The corresponding LT results are shown in Figure 2.7. In order to obtain the best result for a 1 cm defect within the sample, an extra analysis was conducted at 0.01 Hz in a small region of interest (ROI). It must be mentioned that the optimum range of frequencies used for this sample selected based on the results of LT for the first sample as discussed in Section 2.3.1.

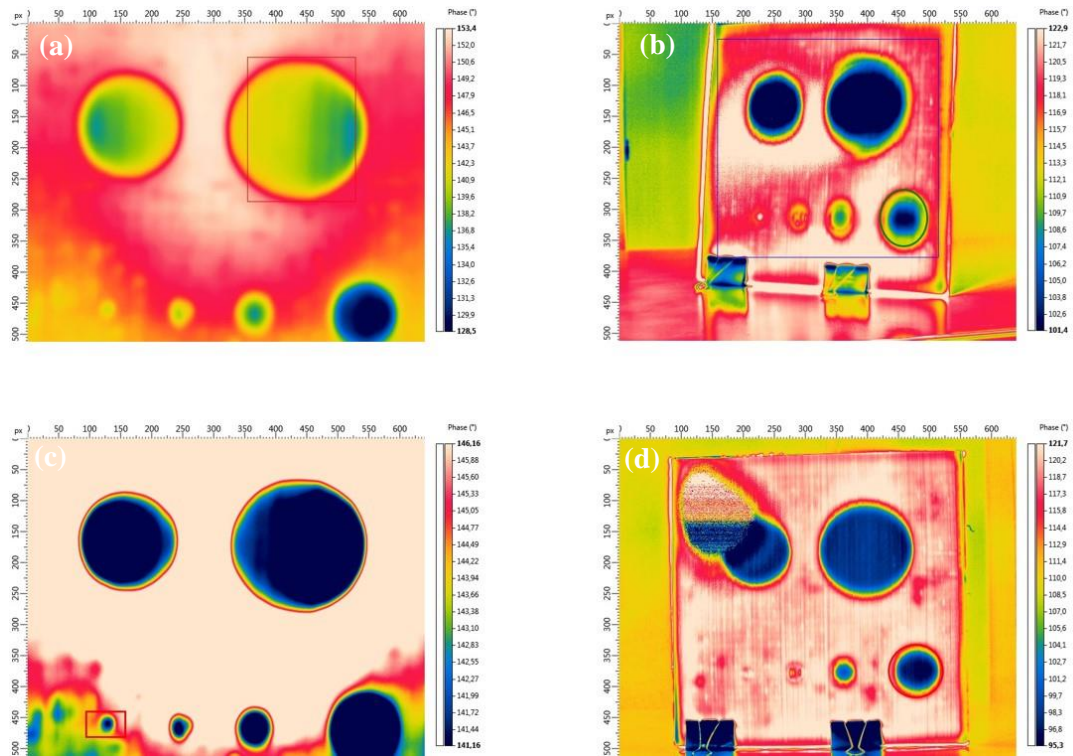


Figure 2.7 LT results of six-hole defects (second sample) with different frequencies (a) 0.01 Hz, (b) 0.02 Hz, (c) 0.01 Hz with different region of interest, (d) 0.05 Hz

Figure 2.7 shows the test result of the six-hole defected sample (second sample). It is seen that the holes with the size of 3 to 6 cm in diameter are clearly visible using any frequency and their boundaries are vivid. However, the location and size of the defects with 1 and 2 cm in diameter are not visible sufficiently when 0.05 Hz and 0.02 Hz frequencies are applied. This uncertainty for small defects can be attributed to the hardware limitation of the thermal camera or the region of interest which is being used for thermal analysis. To overcome this problem using a small region of interest can be helpful, therefore a smaller region of interest is selected at the approximate location of the smallest hole defect as seen in Figure 2.7-(c). This approach helps to identify the exact location and size of the small defect inside the sample. The phase difference between the center of the smallest defect and its surroundings is about 5°, while the phase difference of the entire sample surface as seen in Figure 2.7-(b) is approximately 21°.

The overall analysis of the applied frequencies in the second sample reveals that the optimum LT frequency range is from 0.01 Hz to 0.05 Hz. Using lower frequencies result in higher thermal diffusion length according to Equation 1 (Section 1.2.3.1), and consequently increases the penetration depth of the heat waves inside the material, see

Equation 3 (Section 1.2.3.1). Therefore, with deeper subsurface defects can be detectable using lower frequencies. In other words, the results of LT for sample 2 show that the exact position of the hole-defects can be found with low frequencies since heat propagates homogeneously at low frequency as compared to high frequency.

Apart from the LT tests, PT measurements were also used for the second sample to detect six-hole defects with different sizes inside the material. As can be seen in Figure 2.8, hole defects could be detected by using PT method except for a 1 cm defect. The reason for data loss in small defects, i.e. 1 cm-hole and 2 cm-hole in diameter, can be related to inherent variation in the wavelength of the excitation source, reflection caused by environmental noise and inhomogeneous heating of the material surface.

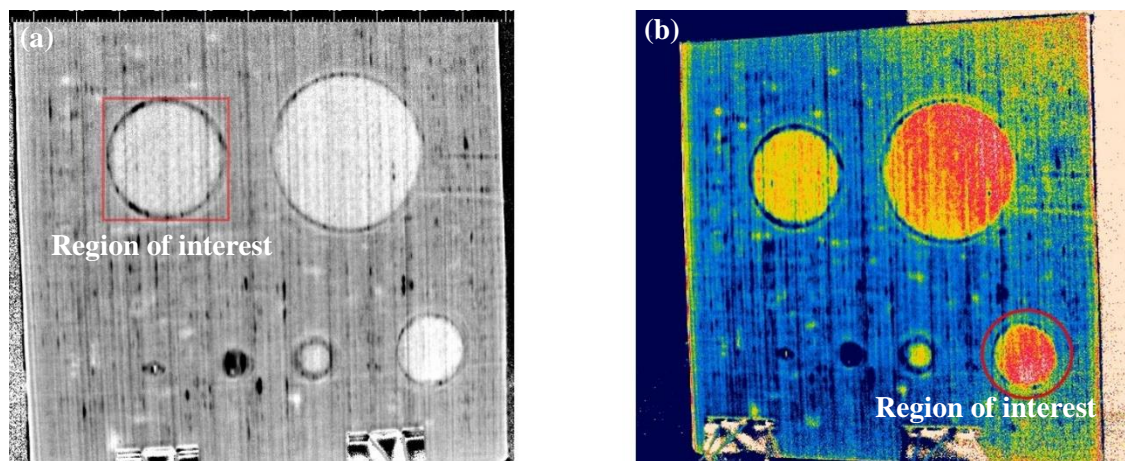


Figure 2.8 PT results of six-hole defects (second sample) (a) 1 Hz flash frequency, (b) 1 Hz flash frequency with different region of interest

2.3.3. Third Sample

LT and PT methods were used to detect and analyze the effect of compressive loading levels namely 15000 N and 3000 N, on CF-based sandwich plate. Since the appearance of the defects are different, appropriate frequencies, sufficient to detect them, were used for LT and PT. As seen in Figure 2.9 and Figure 2.10, damage area as a result of 15000 N is clearly visible through thermal analysis. However, the defect caused by 3000 N is not vivid neither in PT nor LT measurements despite the selection of a smaller region of interest in Figure 2.9-(b) and Figure 2.10-(b). This observation suggests that thermal analysis cannot be used as a sole damage detection method, therefore utilizing a

complimentary assessment method can be advantageous in sandwich structures. More details about this approach are discussed in Chapter 3.

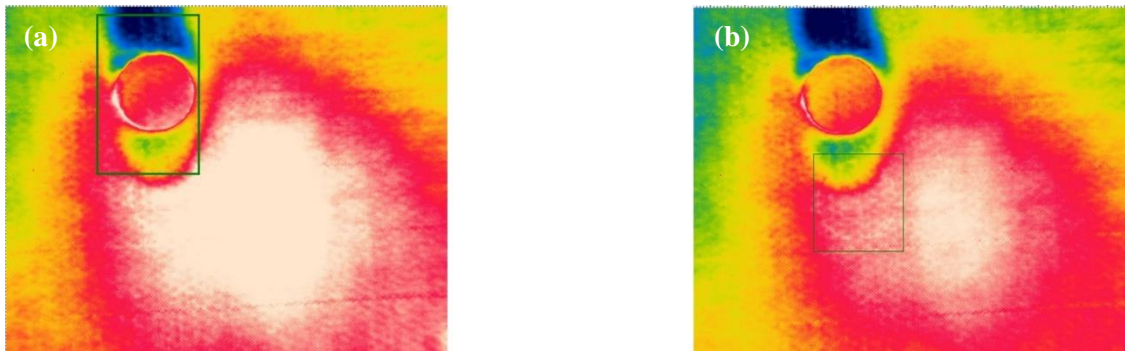


Figure 2.9 LT results of CF sandwich plate after compression test (a) at 0.1 Hz LT frequency focusing 15000 N defect, (b) at 0.1 Hz LT frequency focusing 3000 N defect

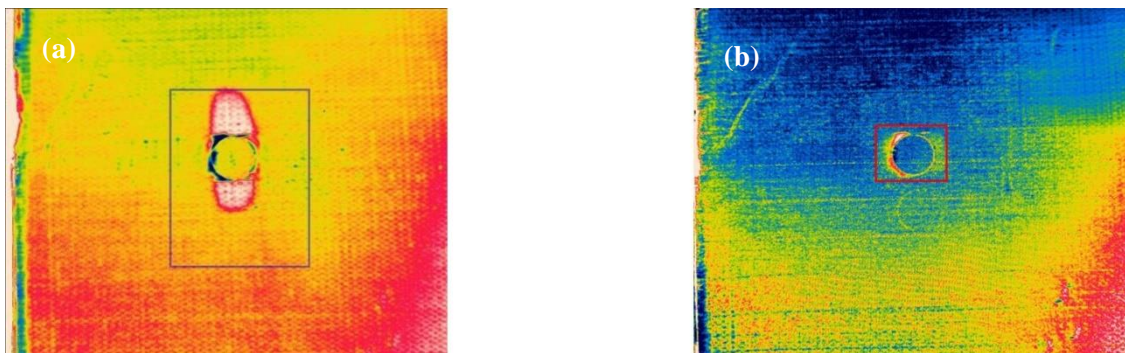


Figure 2.10 PT results of CF sandwich plate after compression test (a) 1 Hz frequency focusing 15000N defect, (b) 5 Hz frequency with different ROI

Chapter 3

In this chapter, honeycomb sandwich panels consisting of highly fire retardant phenolic resin and NomexTM core designed for application in an aircraft cabin interior were investigated by LT and PT techniques. To do so, three different artificial damage modes were created in phenolic resin/glass fiber/ NomexTM honeycomb composites by integration of oil into the honeycomb cells to simulate the liquid ingress, placing a Teflon film between core and face sheet during the manufacturing to create debonding, and using out-of-plane bending of composites to form delamination. The results are presented comparatively based on advantages and disadvantages in terms of capability and detectability of both LT and PT methods.

Apart from the comparison between LT and PT, glass/phenolic honeycomb sandwich structures were subjected to 3-point bending tests with different end-load level. The tests were applied with simultaneous AE registration. In order to compare and verify AE data, LT results are used as they provide better damage characterization as compared to PT method, therefore LT measurements were applied to compare registered AE events during 3-point bending tests.

Non-destructive testing of sandwich structures by active thermography verified with AE

3.1. Experimental

Three different artificial defects were created in phenolic resin/glass fiber based sandwich structures for three different comparisons of evaluating LT and PT. In the first comparison, paraffin oil was embedded into the honeycomb core cells to generate liquid ingress. In the second comparison, Teflon film was placed between the core and face sheet during the manufacturing to create debonding. Lastly, in the third comparison, delamination was formed interior the sample using the out-of-plane bending test.

3.1.1. Phenolic resin/GF/Honeycomb Composite Materials and Manufacturing

Three different specimens were manufactured for comparative experiments. Specimens are made of honeycomb sandwich panels which consist of glass fiber reinforced phenolic

prepreg and 3.2 mm cell size/ 9.65 mm thickness Nomex™ honeycomb core. and processed in a heating press. The representative arrangement of sandwich panels can be seen in Figure 3.1 below:

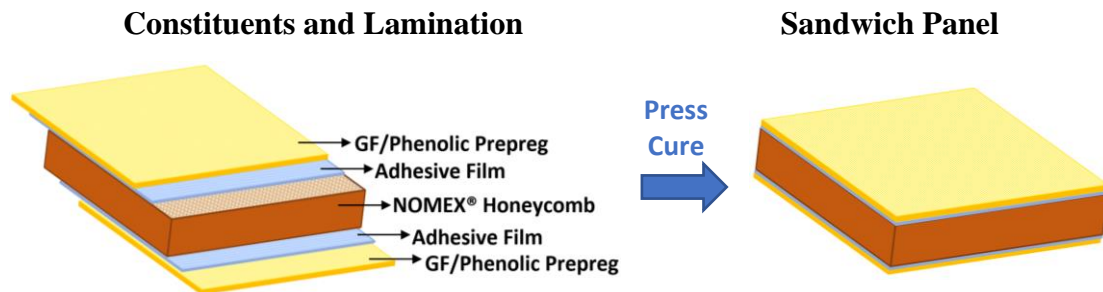


Figure 3.1 Arrangement of sandwich panels during fabrication

In order to compare the efficiency and accuracy of LT and PT, three different artificial defects were created in the sandwich structure during/after manufacturing.

3.1.1.1. First Phenolic Resin Sandwich Sample

The sandwich panels are sensitive for moisture caused by environmental factors and consequently they are susceptible to liquid ingress. This leads to the degradation of the thermo-mechanical properties of the sandwich panels. To simulate this condition, paraffin oil produced by Sigma-Aldrich was embedded in the honeycomb cells before the curing in order to detect the liquid ingress. After curing the material, LT and PT tests were applied separately for the detection of the liquid in the material. A representative image of the defect formation is given in Figure 3.2 below:



Figure 3.2 Representative illustration of embedding paraffin oil in cells before curing

3.1.1.2. Second Phenolic Resin Sandwich Sample

Debonding in sandwich panels might result in core crush and consequently a catastrophic failure. This failure might happen due to defects created during the lay-up of raw materials e.g. wrinkling of the face sheet. They initiate when compressive forces are subjected to the material. Herein, we used a Teflon film between the face sheet and the core during manufacturing to create a debonding on purpose and detect it by LT and PT methods. Representative image of placing Teflon film between face sheet and core is shown in Figure 3.3.

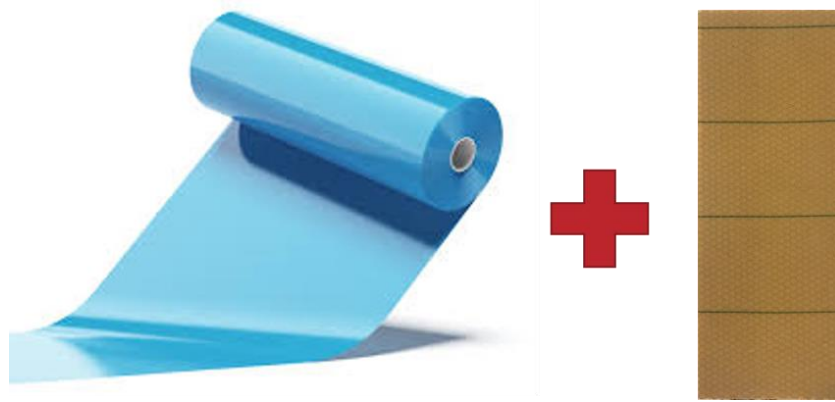


Figure 3.3 A representative illustration of embedding Teflon film into sample to create debonding

3.1.1.3. Third Phenolic Resin Sandwich Sample

One of the most common defects in sandwich panels encountered during the manufacturing, as well as during in-service, is delamination. Since this defect emerged inside the material, it is very difficult to determine with the naked eye. In order to assess the detectability of LT and PT for the delamination, 3-point bending tests with different end load levels were applied onto samples. Sandwich panels were subjected to 3-point bending test based on ASTM C393 [45] standard with Instron 5982 electro-mechanical test machine which described in Chapter 2 (compression test part) and Figure 2.4. The distance between the support spans was 150 mm. A displacement-controlled test was carried out with a displacement rate of 6 mm/min. The representation image of the delamination formation caused by the 3-point bending test is given in Figure 3.4 as below.

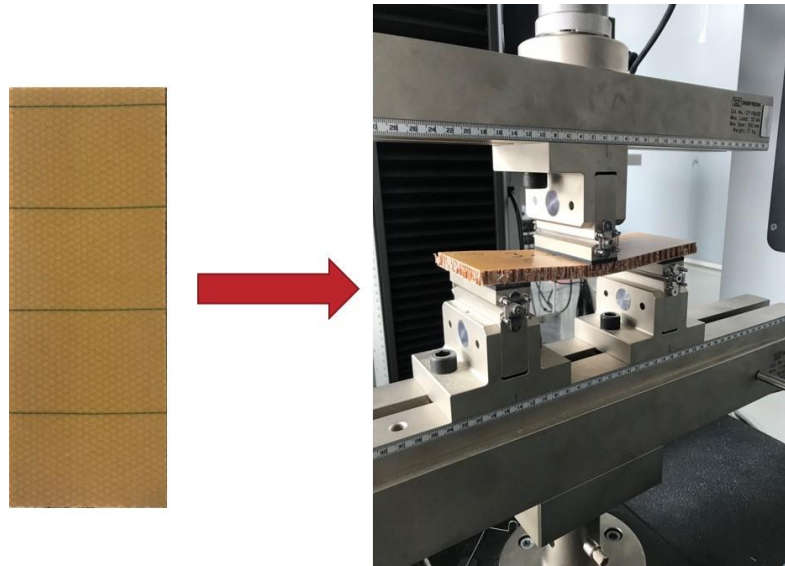


Figure 3.4 Representation of delamination formation

3.2. Experimental Setup for Phenolic Resin Sandwich Samples

3.2.1. Thermography Test Setups

The setup of LT and PT tests is the same as in Chapter 2, and the setup is shown in Figure 3.5 and Figure 3.6. Besides, taking Equation 1 and Equation 3 (Section 1.2.3.1) into consideration for LT method, the depth of the defect in the sample varies according to the frequency of the heat source, i.e. the lower the frequency is given, the deeper the defect is detected. Accordingly, different frequencies were used from 0.1 Hz to 0.002 Hz in order to locate the depth of defects in LT experiments. In particular, very low frequencies were given to the delaminated sample since the damage takes part in very deep (approximately 4 mm). The depth of the defects that can be detected approximately according to the given frequencies is shown in Table 3-1. Furthermore, according to Equation 1 and Equation 3, a correlation between defect depths and frequencies was calculated and it is depicted in Figure 3.7 which will be used as a calibration graph to estimate the defect depth.

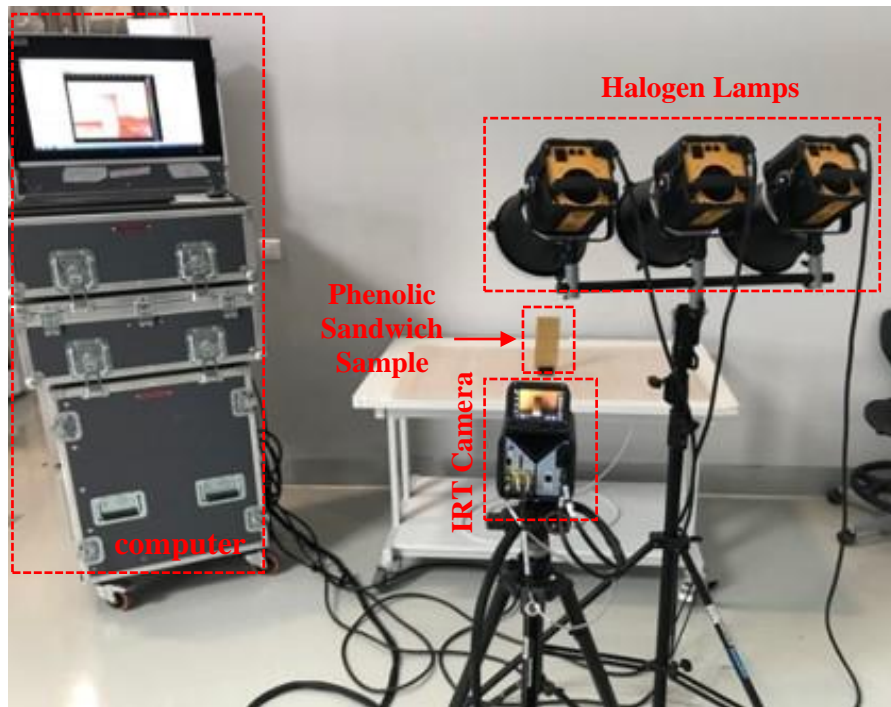


Figure 3.5 LT test set-up for the examination of phenolic sandwich structures

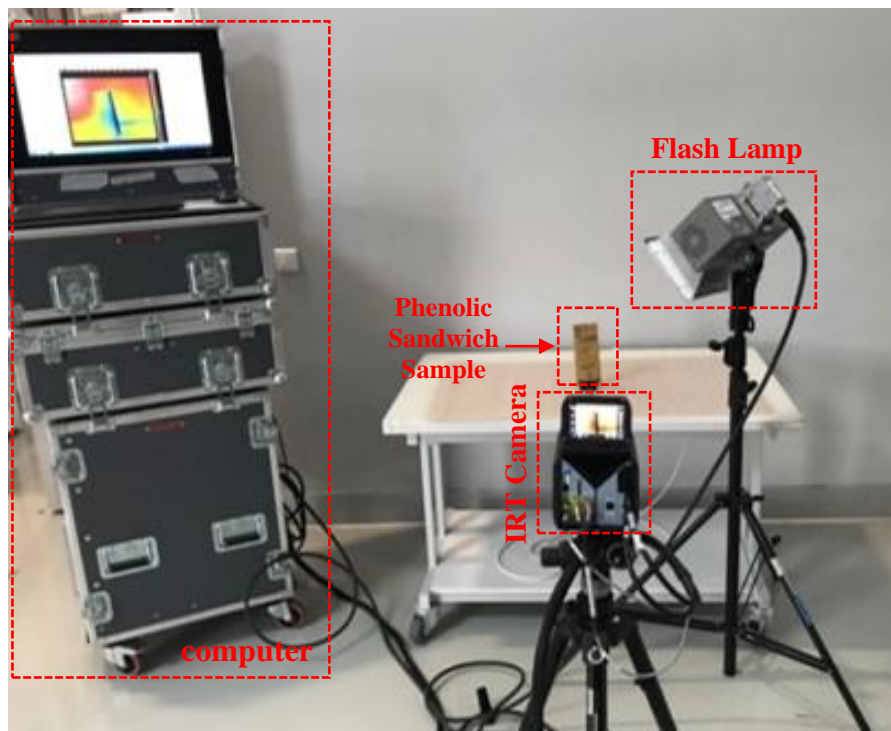


Figure 3.6 PT test set-up for the examination of phenolic sandwich structures

Frequency of Heat Source (Hz)	Depth of Defect (mm)
0.1	1.4163
0.07	1.6928
0.05	2.0029
0.04	2.2393
0.02	3.1669
0.01	4.4787
0.002	10.0147

Table 3-1 Estimated depth of defect at given frequency

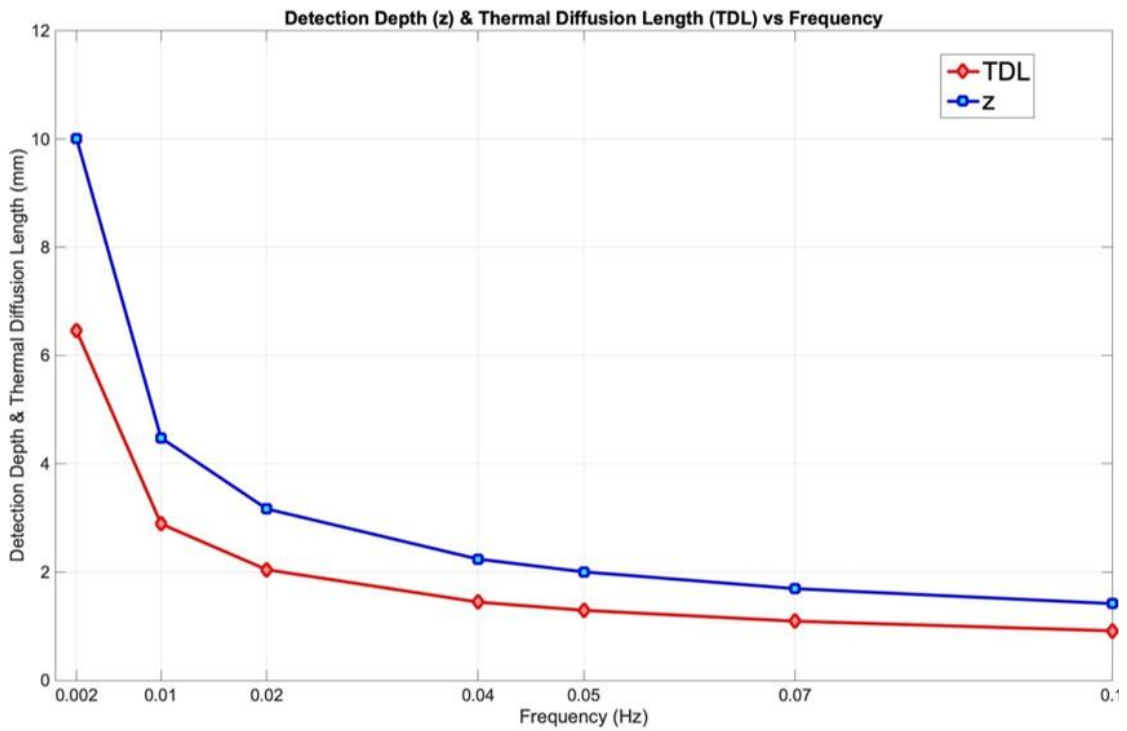


Figure 3.7 Detection depth & thermal diffusion length (mm) vs. modulated frequency

3.2.2. AE Test Setup

AE events during 3-point bending tests were carried out with Mistras PCI 2 acoustic emission apparatus with AEwin PCI2-4 software. Two sensors were placed on the specimen surface during bending tests. The specimen with AE sensors during the bending test is illustrated in Figure 3.8. The sampling rate is 2 MHz for each sensor. Registered AE signals were transformed into digital signals by using Noesis 7 Software to get the frequency domain.

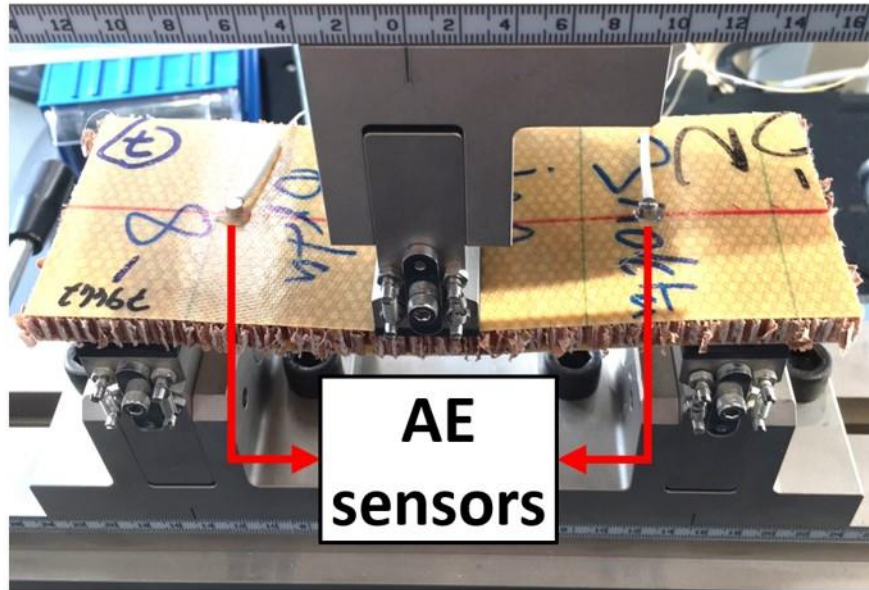


Figure 3.8 Placing AE sensors during 3-point test

3.3. Results and Discussion

3.3.1. Inspection of Liquid Ingress by LT and PT

The pre-embedded paraffin oil inside the honeycomb core cells could be detected in both LT and PT methods. Selected results are depicted in Figure 3.9, Figure 3.10 and Figure 3.11, and the rounded regions indicate the liquid ingress location in the material.



Figure 3.9 Raw image of LT for liquid ingress test in sandwich composite

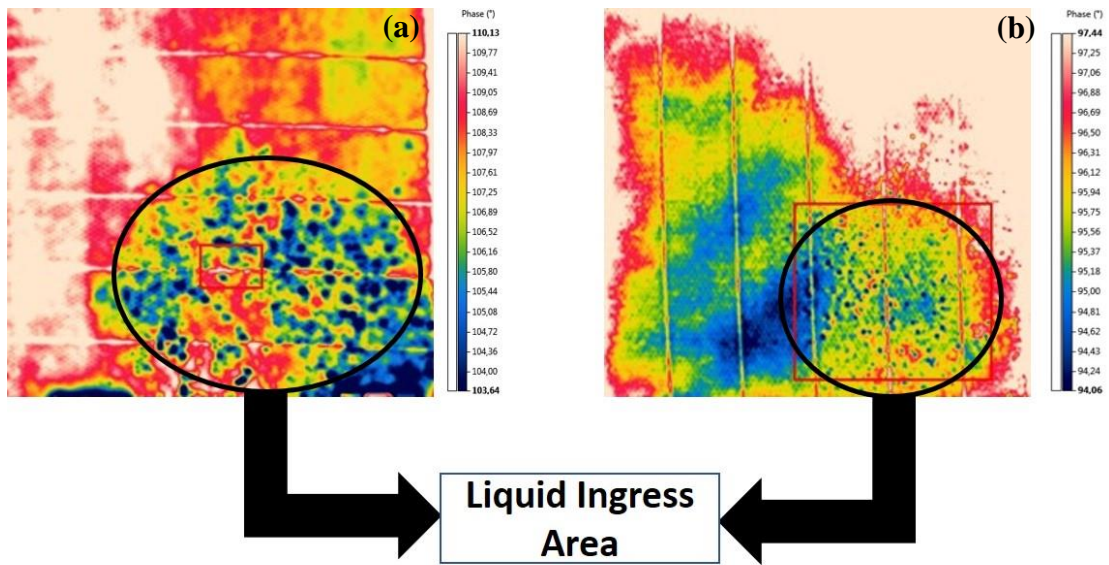


Figure 3.10 LT images: (a) at frequency of 0.01 Hz and (b) at frequency of 0.05 Hz for liquid ingress test in sandwich composite

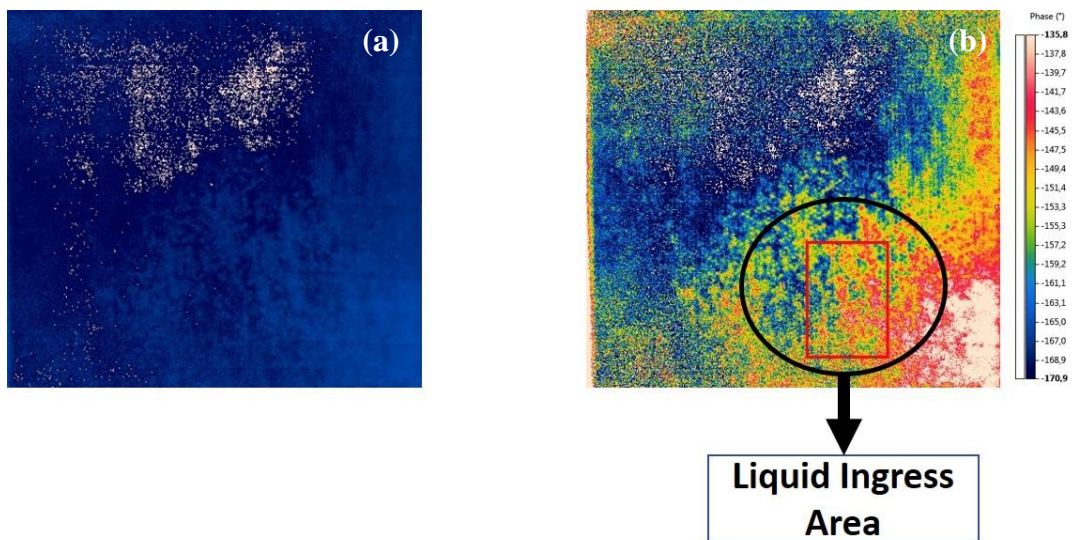


Figure 3.11 PT images: (a) raw image and (b) at frequency of 1 Hz for liquid ingress test in sandwich composite

In the liquid ingress sample as presented in Figure 3.9, Figure 3.10 and Figure 3.11, both LT and PT methods could detect the pre-embedded Paraffin oil inside the honeycomb core cells. In the circled region in Figure 3.10 and Figure 3.11, blue spots and their

surrounding are present the liquid in the sample. The LT approach provides a clearer and sharper visualization of the defect, this clarity is related to the energy deposited onto the surface of the test specimen with a heat source having a single frequency in LT. In other words, the area of liquid ingress in the sample is clearly detectable due to equal and sufficient energy with the usage of a single frequency, i.e. all heat sources convey the same signal simultaneously over the same frequency channel. Moreover, the liquid ingress region in the sample could be obtained with different frequencies (e.g. 0.01 Hz and 0.05 Hz), see Figure 3.10. However, Figure 3.10-(a) gives the more explicit and clearer result as compared with Figure 3.10-(b) since the heat is distributed more homogeneously on the sample, i.e. the lower the frequency the deeper the heat penetration. This result also corresponds to the estimated depth of defect at given frequency as given in Table 3-1. According to Table 3-1, if a frequency of 0.01 Hz is applied, a defect of 4.4787 mm depth is detected, and/or if a frequency of 0.05 Hz is applied, a defect of 2,0029 mm depth is detected. Therefore, it is seen that the liquid ingress is about 4.5 mm deep in the sample as can be seen in Figure 3.10-(a). On the other hand, although liquid in the sample was detected by PT after applying FT to the raw image, the results are not as explicit as LT. The reason for this, the energy deposited on the surface of the test material by using flash as a heat source causes reflections and non-homogenous heating in the material at different frequencies.

3.3.2. Inspection of Debonding by LT and PT

Debonding can be clearly observed by both LT and PT methods. The results are as indicated in Figure 3.12 to Figure 3.15. They present the detection of Teflon film in the enframed region.

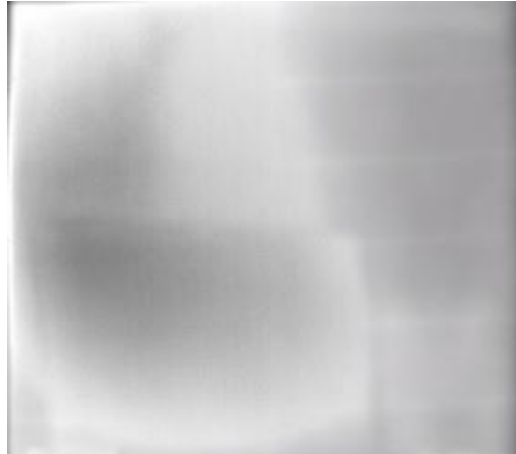


Figure 3.12 Raw image of LT for debonding in sandwich composite

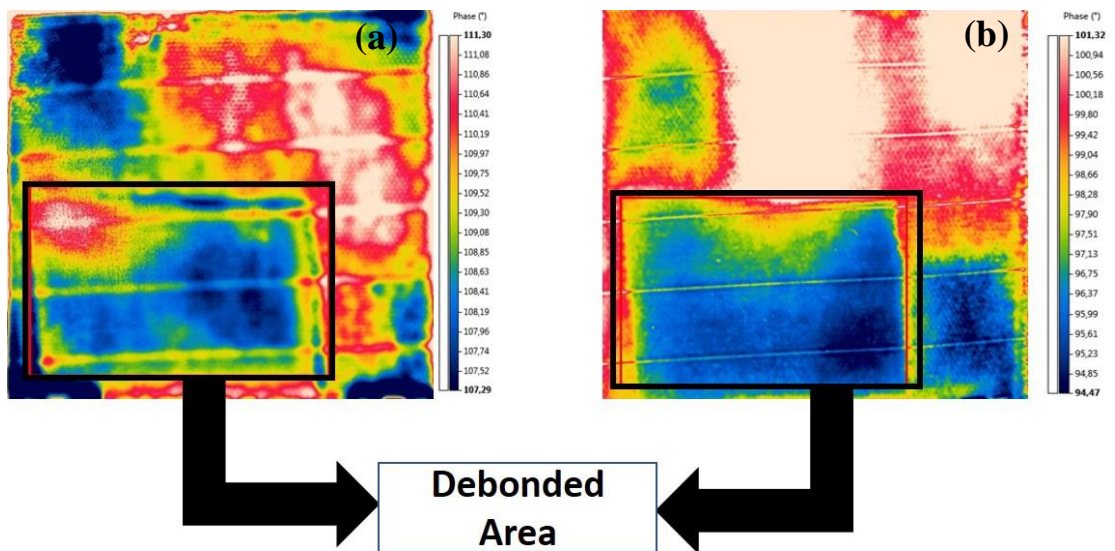


Figure 3.13 LT images: (a) at frequency of 0.01 Hz and (b) at frequency of 0.07 Hz for debonding in sandwich composite

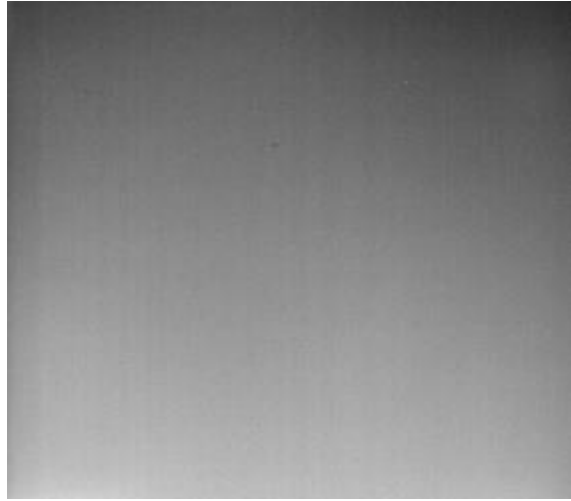


Figure 3.14 Raw image of PT for debonding in sandwich composite

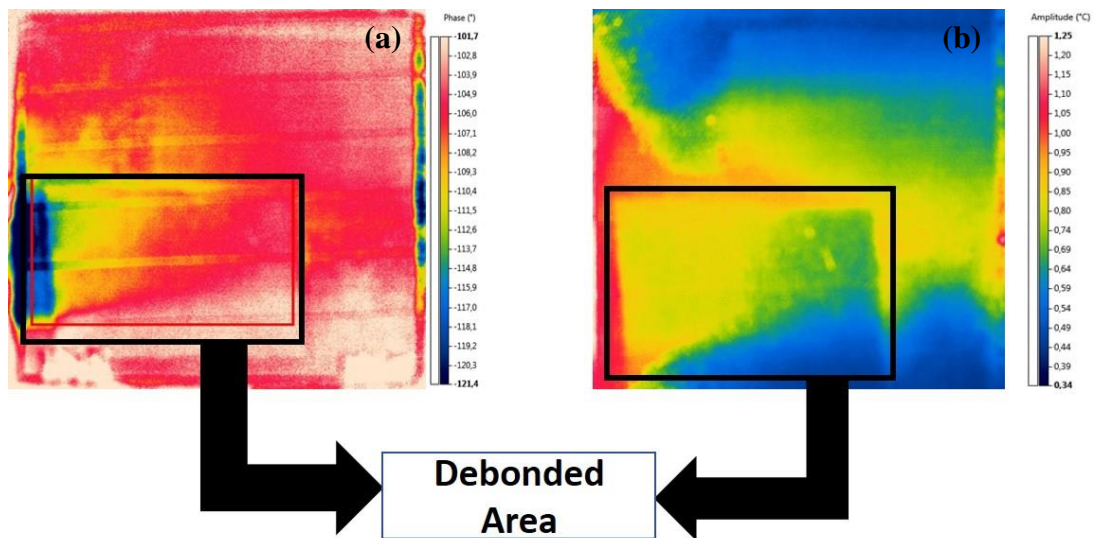


Figure 3.15 PT images: (a) at frequency of 1 Hz (phase mode) and (b) at frequency of 1 Hz (amplitude mode) for debonding in sandwich composite.

For the second specimen with Teflon film between the face sheet and the core, i.e. artificial debonding, can clearly be detected by both PT and LT methods as shown in Figure 3.13 and Figure 3.15. In this defect type, LT method provided better insight into the internal damage compared to PT even in higher frequency, because the damage emerged in the subsurface of the sample. Since there is a possibility of controlling the thermal exposure of the specimen surface in terms of intensity in LT technique, a better result for the subsurface defect is obtained. On the other hand, PT suffers from non-uniform exposure and non-uniform heating due to emissivity variations. Despite these

disadvantages of PT method, debonding close to the subsurface of the sample could be detected, especially amplitude mode in Figure 3.15-(b).

3.3.3. Inspection of Delamination by LT and PT

Samples were examined by LT and PT on defective and non-defective surfaces after out-of-plane bending. However, damage boundaries were determined only by the LT method when examined from the non-defective side. Selective results analyzed from the non-defective side are exhibited in Figure 3.16 and Figure 3.17.

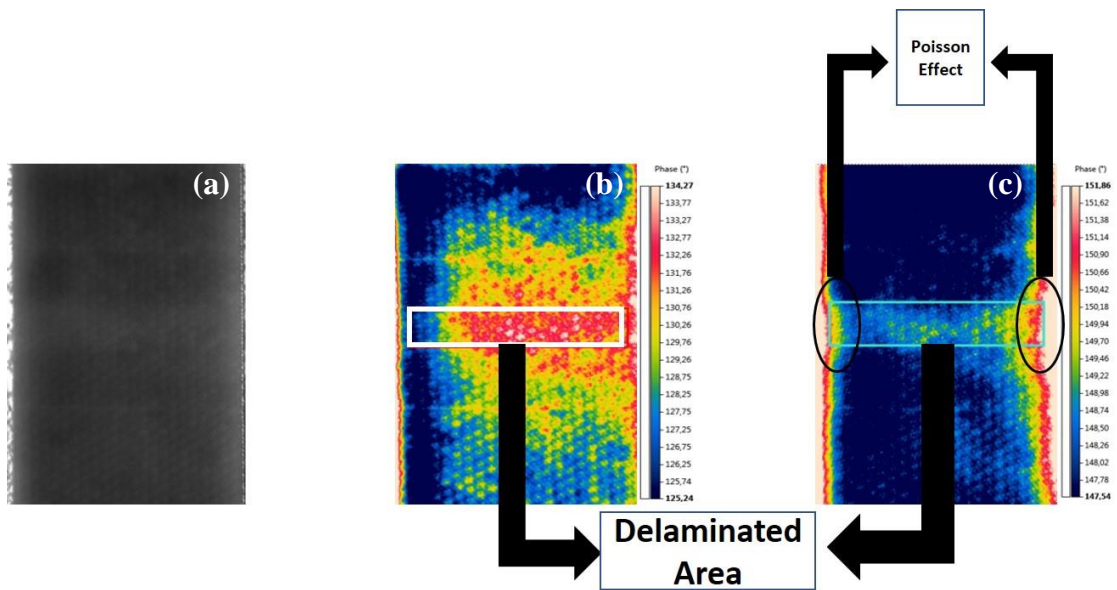


Figure 3.16 LT images: (a) raw image, (b) at frequency of 0.01 Hz, c) at frequency of 0.002 Hz for 3-point bending test in sandwich composite captured from non-defective side

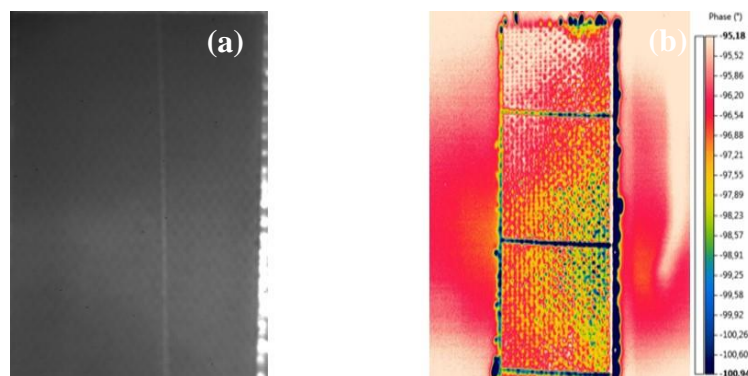


Figure 3.17 PT images: (a) raw image, (b) at frequency of 1 Hz for 3-point bending test in sandwich composite captured from non-defective side

Comparing the results recorded by IR camera in Figure 3.16 and Figure 3.17, one can easily say that LT is able to detect delamination in phase image from non-defective region. Since the phase image in LT is relatively independent from the optical and thermal surface properties, the detected defect is most clearly visible in phase mode. Here, LT method provides a more accurate view on damage boundaries, and with higher precision to detect the damage depth compared to PT. Moreover, LT reveals the different defects formed after bending in the vicinity of the sample. To get a comprehensive understanding of the damage at a different depth of specimen various frequencies were applied based on the estimation made by Equation 1 and Equation 3 in Chapter 1, and the corresponding estimated depths of defects according to the applied frequencies are shown in Table 3-1 and Figure 3.7. In particular, the delamination resulting from the out-of-plane bending test in the sample of Figure 3.16-(c) is approximately 10 mm deep and this depth is determined if 0.002 Hz modulated-frequency is applied in LT. This observation verifies the estimated damage depths according to the applied modulation frequency shown in Table 3-1 and Figure 3.7. Furthermore, it can be clearly seen that the Poisson effect after the test caused by bending load can be detected in Figure 3.16-(c) if very low frequency is applied. Hence, it can be said that the effect of modulation frequency on the depth of detected damages was validated by other experimental methods. It can be concluded that lower frequency reveals information of damage at higher depth while higher frequencies provide information closer to the surface of the specimen.

3.3.4. Comparison of AE with LT

In order to make a correlation between the AE results and thermography inspections of induced damage modes, tests were interrupted at 4 different levels. Only one test was performed until the final fracture. All tested specimens were compared with a reference sample that was not tested. Four interruption levels are marked as shown in Figure 3.18.

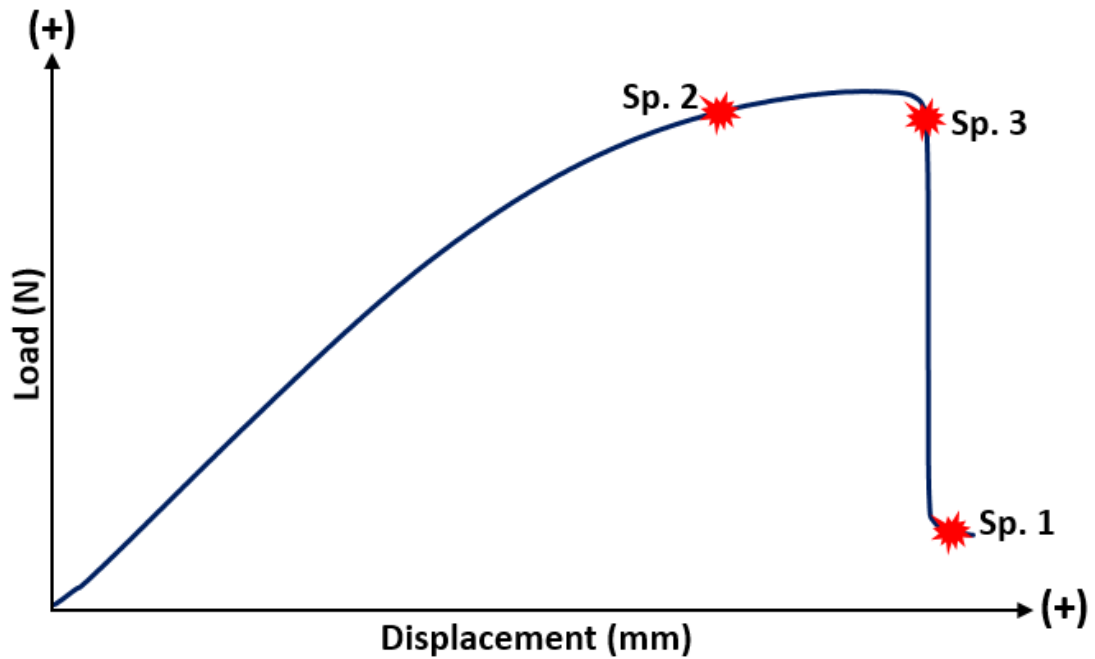


Figure 3.18 Test interruption levels of specimens with respect to Load vs. Displacement diagram

AE registrations applied onto samples during 3-point bending, and they were examined by LT on defective and non-defective surfaces after 3-point bending. The reference sample which was not undergone the test is shown in Figure 3.19. Selective results analyzed by LT after the tests and the data obtained from the AE sensors during the tests are shown in Figure 3.20 to Figure 3.22.

The results of the complete fracture are presented first in Figure 3.20. Large delaminations and complete fracture through the width of the specimen are obvious in Figure 3.20. Registered AE signals are presented with two different parameters. The first one is cumulative AE energy. It can be seen that damage initiation starts at around 520 N. It cumulates sharply until 700 MPa, then the slope of the cumulative AE energy curve decreases. In the end, the slope becomes a plateau with a large load drop. In addition to this, the amplitude is used to present damage accumulation throughout the test. It is seen that the average amplitude values increase as the load increases. Damage progression can be interpreted as follow: low amplitude levels could be registered due to matrix cracks in the face sheets, then an increasing number of cracks can cause higher amplitude signals.

The interpretations can be extended but most of them would remain as interpretations only. In order to make a reliable explanation for damage progression, AE results of interrupted tests are explained with LT measurements. A fully fractured sample can be seen in Figure 3.20-(c) to Figure 3.20-(f) in LT where various wave properties are utilized to detect structural inhomogeneities. As seen in LT results in Figure 3.20, damage boundary and size caused by fracture are clearly seen. Apparent damage progress in Figure 3.20 can be as follow:

1. Damage initiation and accumulation in facesheets in the form of matrix cracking, fiber/matrix interphase failure.
2. Delamination between facesheet and honeycomb core
3. Abrupt failure in honeycomb cells
4. Fiber breakage through the width of the specimen

The aforementioned failure steps are speculations based on visual observations. In order to make a reliable assessment, results of interrupted tests are analyzed in detail.

Results of the first interruption are presented in Figure 3.21. Damage initiation occurs at a displacement of 2.1 mm as seen in Figure 3.20. AE signals with very low-level amplitude values are registered as can be seen in Figure 3.21-(b). LT measurements show a significant difference in the material structure before and after 3-point bending test as seen in Figure 3.19 and Figure 3.21, respectively. This difference is not visible for naked-eye, however, using thermal analysis indicates that a remarkable structural inhomogeneity in the middle of the sample has occurred. This is the region where the loading span of test fixture has been applied. Comparison of these images with the results of delamination and debonding in Sections 3.3.2 and 3.3.3 indicates that the severity of the damage for the current case is lower. Thus, damage modes with lower amplitude, seen in Figure 3.21-(b), such as matrix cracking must have caused structural variations in Figure 3.21-(c) to Figure 3.21-(e). The occurrence of matrix cracking at load level at initial stages of the test causes a reduction in through-the-width strains, and this is the Poisson effect, detected by LT. Normally, this type of deformation gradients can be clearly detected by in-situ measurement techniques, such as DIC. However, the test setup of 3-point bending does not allow to apply DIC from the top view, so that post-mortem LT measurement can successfully detect this deformation in Figure 3.21-(c) to Figure 3.21-(e). Moreover, the result of damage caused by 3000 N in Section 2.3.3 indicated that

the thermal analysis could not effectively detect less severe failures in sandwich structures. Since matrix cracking is usually associated with minor failures in material, the disability of thermography to locate them precisely must be taken into account.

The next test is stopped immediately at the beginning moment of the final load drop in Figure 3.22. This specimen shows initial damage onset at 2.2 mm displacement which is very similar to previous samples. Very close damage initiation conditions as determined by AE technique show that the tests are consistent and replicable. The gradual increase and evolution of amplitude for AE hits in Figure 3.22-(b) is like the one in Figure 3.20-(b), therefore it can be assumed that a similar damage progression occurs in this specimen as well. LT image in Figure 3.22-(c) shows a highly out-of-phase region just at the midpoint of the sample which implies delamination between the facesheet and honeycomb core. These results are consistent with the observation in delamination and debonding in Sections 3.3.2 and 3.3.3. So far one can conclude that load drop occurs due to delamination between the facesheet and the core, and this brings out fiber breaks which were seen in Figure 3.20. This assumption was also confirmed by visual inspection of the surface of samples where no sign of fiber failure was seen at least on a macro level.

Single AE parameters can be used to interpret the damage modes as seen here. On the other hand, the application of clustering algorithms to the registered AE data can provide better insight for correlation with damage modes. The next step will be the clustering of these data with k-means++ clustering algorithm. This is left for the future work of this study.

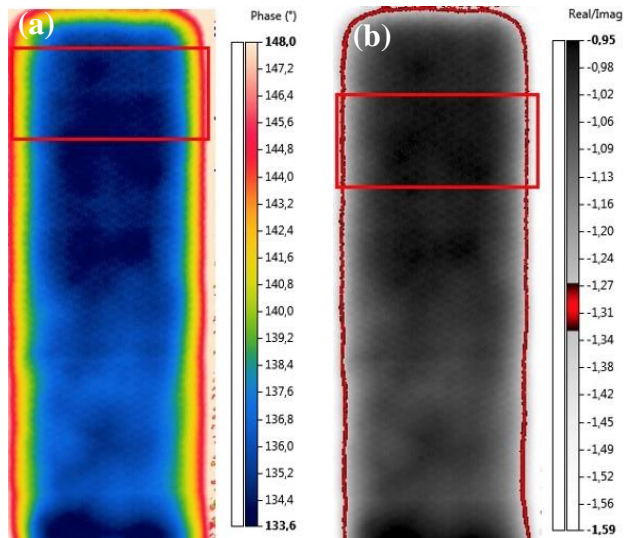


Figure 3.19 The LT results of reference sample (untested): (a) FT at front image frequency of 0.002 Hz (phase rain mode), (b) front image frequency of 0.002 Hz (real/imag iron mode)

0.002 Hz, which is very low, LT frequency was applied to the sample shown in Figure 3.19 in order to compare with tested samples. As can be seen in both Figure 3.19-(a) and Figure 3.19-(b) there is no defect and damage boundary in the sample.

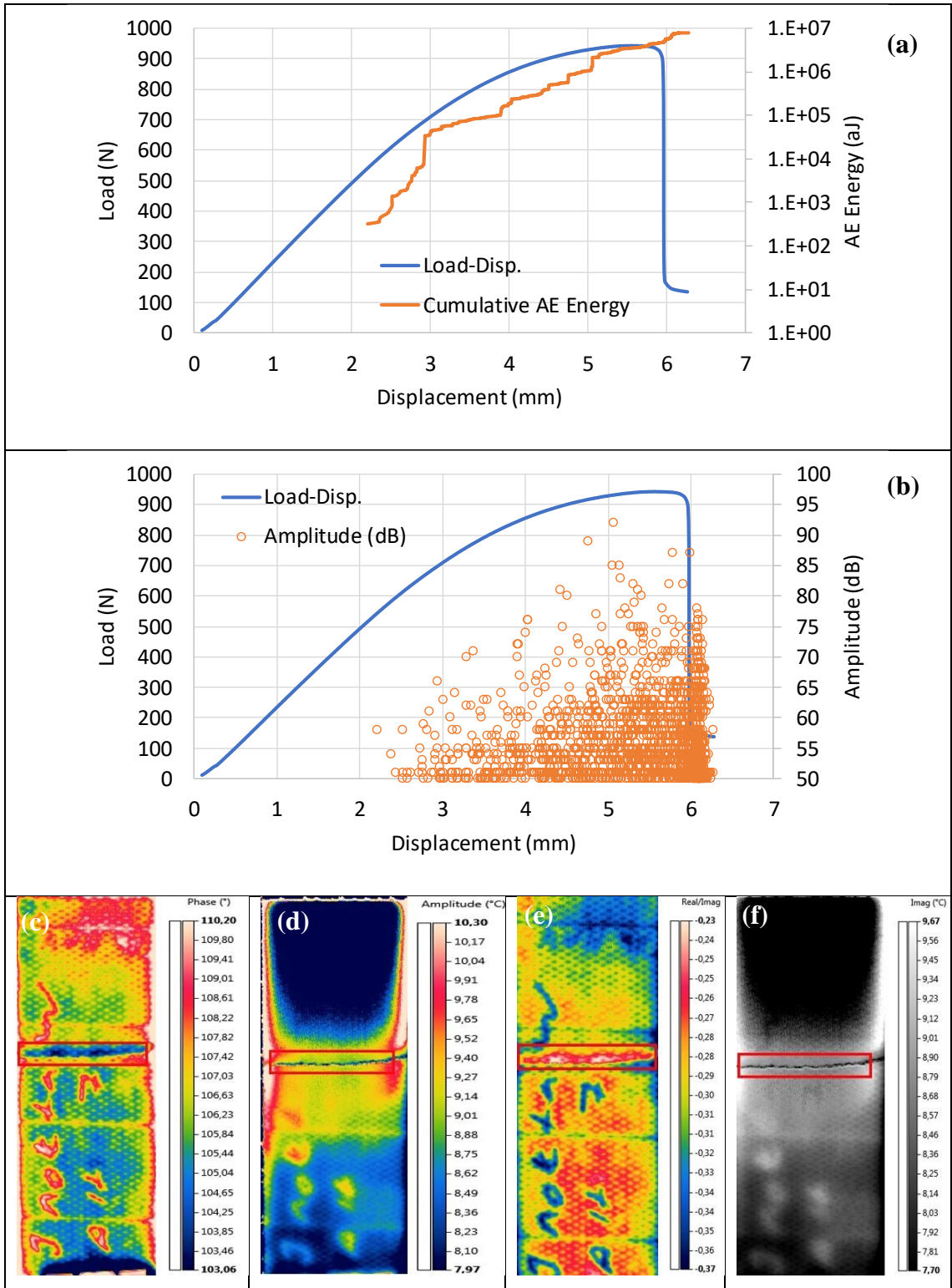


Figure 3.20 AE and LT results of Sample 1: (a) cumulative AE energy, (b) average amplitude values of AE, (c) front image frequency of 0.01 Hz (phase rain mode), (d) front image frequency of 0.01 Hz (amplitude rain mode), (e) front image frequency of 0.01 Hz (real/imag rain mode), (f) front image frequency of 0.01 Hz (imag default mode)

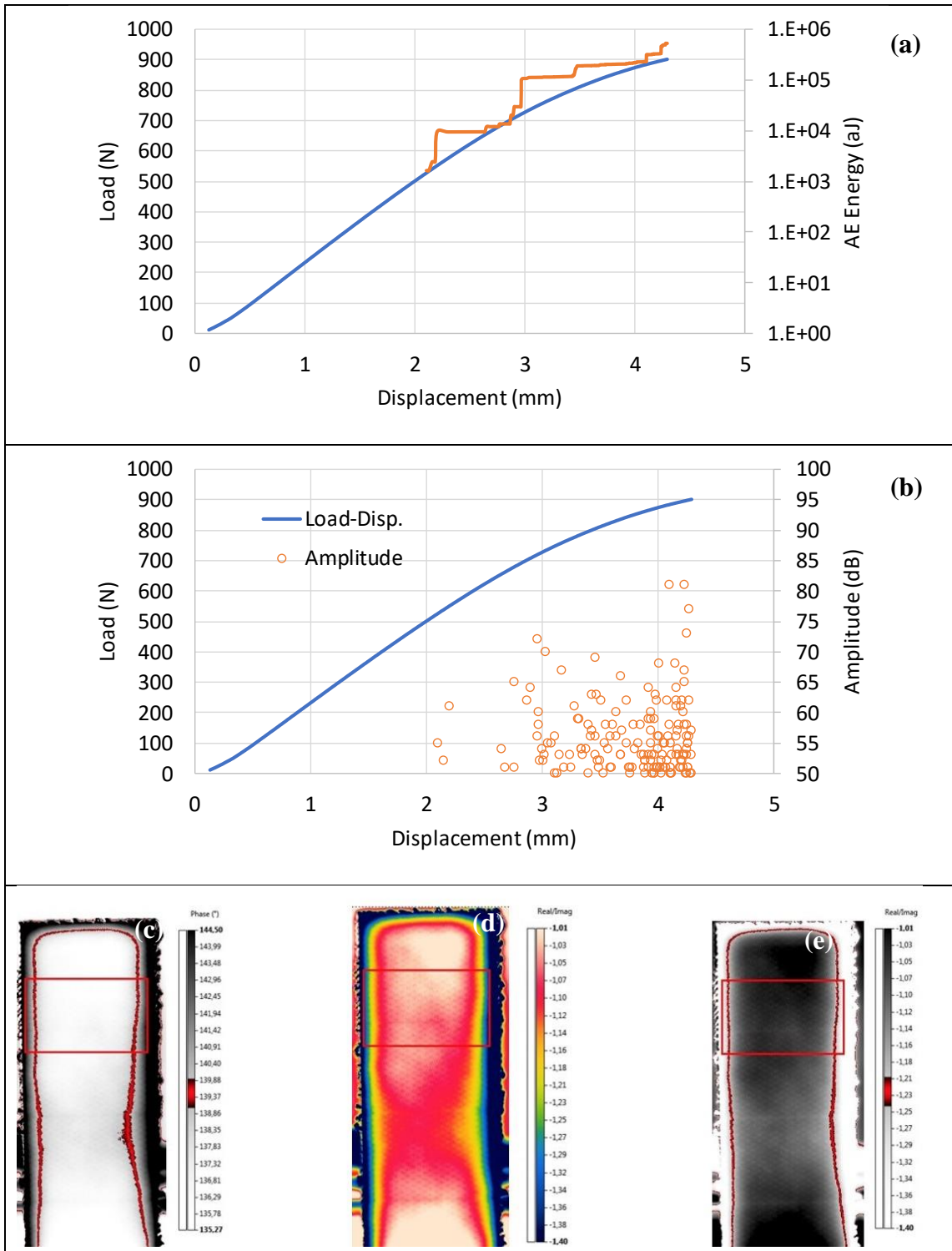


Figure 3.21 AE and LT results of Sample 2 (a) cumulative AE energy, (b) average amplitude values of AE, (c) front image frequency of 0.002 Hz (phase iron mode), (d) rear image frequency of 0.002 Hz (real/imag rain mode), (e) rear image frequency of 0.002 Hz (real/image)

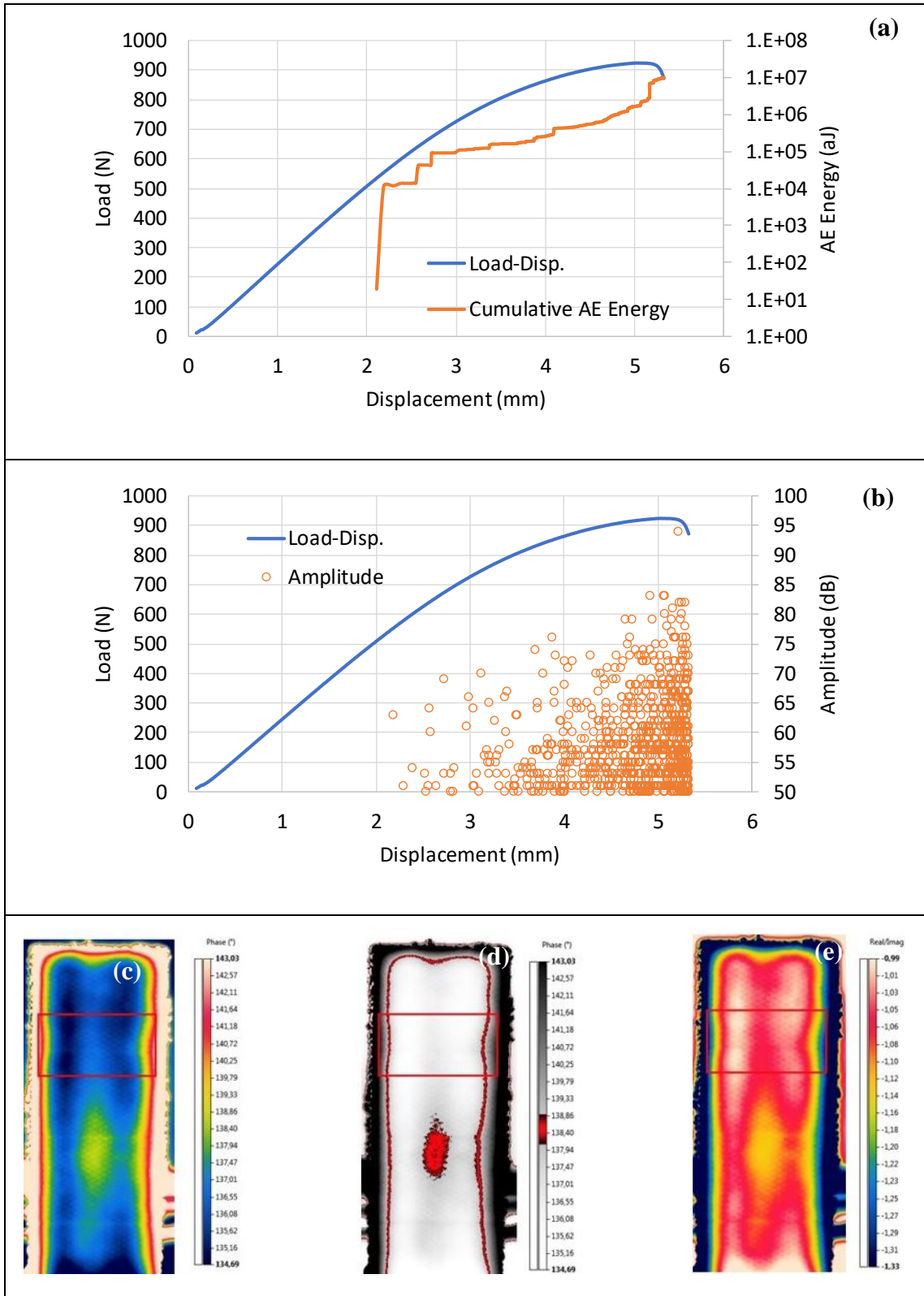


Figure 3.22 AE and LT results of Sample 3: (a) cumulative AE energy, (b) average amplitude values of AE, (c) front image frequency of 0.002 Hz (phase rain mode), (d) front image frequency of 0.002 Hz (phase iron mode), (e) rear image frequency of 0.002 Hz (real/imag rain mode)

Chapter 4

CONCLUSIONS

In Chapter 2, in the first experiment, two-hole defects on the carbon fiber plate (first sample) were successfully determined by lock-in thermography method and the temperature differences due to the hole-defects in the sample were examined. The results indicated that the selection of appropriate frequencies in LT measurements could alter the detectability of hole defects. In the second experiment, the effective choosing small region of interest to identify the location of small hole defects was shown. Moreover, the advantage of using LT in comparison with PT was presented experimentally in identifying small defects inside the composite material. In the compression test of sandwich CF sample, the larger defect caused by the 15000 N compression force and the damage boundaries caused by the defect were determined by two thermography methods. However, the smaller damage caused by the 3000 N compression force was not characterized effectively. Therefore, it was shown that the severity of damage has a direct relationship with the ability of thermal analysis measurement, which requires complementary damage assessment through other methods like AE.

In Chapter 3, a honeycomb sandwich composite structures with various damage types were inspected by LT and PT techniques. Both methods demonstrated the capability to detect various damages in the structure. In particular;

- In the liquid ingress test, despite fast and easy use of PT, a clearer and sharper visualization image was provided by LT. This superiority of LT is attributed to more effective transfer energy from heat source to the material and consequent penetration into the layered structure of the sample.
- A similar result from the second specimen with Teflon film between the face sheet and the core is obtained. Thus, LT provides more accurate and clearer information on the damage state of debonding.
- In the delaminated sample, the LT method provides a more accurate view of the boundaries of damage and provides a higher sensibility to detect the depth of

damage compared to PT. In particular, only LT method is able to detect the delaminated region after out-of-plane bending from the non-defective side of the specimen. This result shows the advantage of LT as compared to PT measurement in structural health monitoring of thick samples due to the possibility of using very low frequency assessment (0.002 Hz in this investigation). Taking Equation 1 and Equation 3 into consideration for LT method, the depth of the defect in the sample varies according to the frequency of the heat source, i.e. the lower the frequency is given, the deeper the defect is detected.

Correlation of AE data with LT measurement for different end-loads in Section 3.3.4 shows that:

- Four failure steps can be identified for sandwich panels namely matrix and fiber/matrix interphase failure, facesheet/core delamination, core fracture and facesheet fiber breakage.
- Comparison of samples before and after 3-point bending tests reveals that lock-in thermography can be used to locate structural inhomogeneity despite lack of macro damages. Structural inhomogeneities without any visible marks on the sample are probably related to matrix cracking of the facesheet.
- Delamination between facesheet and honeycomb core in the material is obviously detectable by LT analysis just before abrupt failure in load value. This delamination between the components of sandwich structure suggests that fiber breakage as the last stage of material failure is inhibited due to sudden loss of material integrity and consequent removal of load from the test instrument.

This study demonstrated that the deeper view on how LT and PT can be correlated to the different damage types and different damage depths. Last but not least, various damage modes of carbon fiber reinforced polymeric composites and phenolic based sandwich structures used in aircraft parts were characterized by this study. Thus, this study has a great contribution in the development of structural health monitoring systems to assess the damage modes that are characterized for these materials.

REFERENCES

- [1] A. Katunin, K. Dragan, and M. Dziendzikowski, "Damage identification in aircraft composite structures: A case study using various non-destructive testing techniques," *Compos. Struct.*, 2015.
- [2] H. Zhang *et al.*, "Optical excitation thermography for twill/plain weaves and stitched fabric dry carbon fibre preform inspection," *Compos. Part A Appl. Sci. Manuf.*, 2018.
- [3] H. Zhang *et al.*, "An experimental and analytical study of micro-laser line thermography on micro-sized flaws in stitched carbon fiber reinforced polymer composites," *Compos. Sci. Technol.*, 2016.
- [4] F. Campbell, *Manufacturing Technology for Aerospace Structural Materials*. 2006.
- [5] C. Ibarra-Castanedo and X. Maldague, "Pulsed phase thermography reviewed," *Quantitative InfraRed Thermography Journal*. 2004.
- [6] C. Ibarra-Castanedo, L. Brault, M. Genest, V. Farley, and X. P. V. Maldague, "Detection and characterization of water ingress in honeycomb structures by passive and active infrared thermography using a high resolution camera," 2012.
- [7] "Gurit completes aerospace qualification," *Reinforced Plastics*. 2017.
- [8] Gurit, "Aerospace Prepreg Brochure." [Online]. Available: <https://www.gurit.com/-/media/Gurit/Datasheets/aerospace-prepreg-brochure.pdf>.
- [9] J. Seyyed Monfared Zanjani, B. Saner Okan, P. N. Pappas, C. Galiotis, Y. Z. Menciloglu, and M. Yildiz, "Tailoring viscoelastic response, self-heating and deicing properties of carbon-fiber reinforced epoxy composites by graphene modification," *Compos. Part A Appl. Sci. Manuf.*, 2018.
- [10] F. E. Oz, N. Ersoy, and S. V. Lomov, "Do high frequency acoustic emission events always represent fibre failure in CFRP laminates?," *Compos. Part A Appl. Sci. Manuf.*, 2017.
- [11] M. Genest *et al.*, "Comparison of Thermography Techniques for Inspection of F / A-18 Honeycomb Structures," *Aircr. Aging 2007 Conf.*, 2007.
- [12] J. Kastner, E. Schlotthauer, P. Burgholzer, and D. Stifter, "Comparison of x-ray computed tomography and optical coherence tomography for characterisation of glass-fibre polymer matrix composites," *World Conf. Non-destructive Testing*,

August 30 – Sept. 3, 2004.

- [13] D. J. Bull, S. M. Spearing, I. Sinclair, and L. Helfen, “Three-dimensional assessment of low velocity impact damage in particle toughened composite laminates using micro-focus X-ray computed tomography and synchrotron radiation laminography,” *Compos. Part A Appl. Sci. Manuf.*, 2013.
- [14] F. Aymerich and S. Meili, “Ultrasonic evaluation of matrix damage in impacted composite laminates,” *Compos. Part B Eng.*, 2000.
- [15] Y. Y. Hung and H. P. Ho, “Shearography: An optical measurement technique and applications,” *Materials Science and Engineering R: Reports*. 2005.
- [16] C. Garnier, M.-L. Pastor, F. Eyma, and B. Lorrain, “The detection of aeronautical defects in situ on composite structures using Non Destructive Testing,” *Compos. Struct.*, 2011.
- [17] X. Maldague and S. Marinetti, “Pulse phase infrared thermography,” *J. Appl. Phys.*, 1996.
- [18] C. Ibarra-Castanedo and X. Maldague, “Pulsed phase thermography reviewed,” *Quant. Infrared Thermogr. J.*, 2004.
- [19] J. Renshaw, J. C. Chen, S. D. Holland, and R. Bruce Thompson, “The sources of heat generation in vibrothermography,” *NDT E Int.*, 2011.
- [20] A. Ataş and C. Soutis, “Subcritical damage mechanisms of bolted joints in CFRP composite laminates,” *Compos. Part B Eng.*, 2013.
- [21] L. Cheng and G. Y. Tian, “Surface crack detection for carbon fiber reinforced plastic (CFRP) materials using pulsed eddy current thermography,” *IEEE Sens. J.*, vol. 11, no. 12, pp. 3261–3268, 2011.
- [22] J. García-Martín, J. Gómez-Gil, and E. Vázquez-Sánchez, “Non-destructive techniques based on eddy current testing,” *Sensors*. 2011.
- [23] Olympus IMS, “Nondestructive Bond Testing for Aircraft Composites.” [Online]. Available: <https://www.olympus-ims.com/en/applications/non-destructive-bond-testing-aircraft-composites/347-pos.88.html>.
- [24] W. Ben Larbi, C. Ibarra-Castanedo, M. T. Klein, A. Bendada, and X. P. V. Maldague, “Experimental Comparison of Lock-in and Pulsed Thermography for the Nondestructive Evaluation of Aerospace Materials,” in *6th Int’ernational Workshop-NDT Signal Processing ASPNDE 2009*, 2009.
- [25] Y. Duan, S. Huebner, U. Hassler, A. Osman, C. Ibarra-Castanedo, and X. P. V. Maldague, “Quantitative evaluation of optical lock-in and pulsed thermography

- for aluminum foam material,” *Infrared Phys. Technol.*, 2013.
- [26] S. Gholizadeh, “A review of non-destructive testing methods of composite materials,” *Procedia Struct. Integr.*, vol. 1, pp. 50–57, 2016.
- [27] M. Ishikawa, M. Ando, M. Koyama, and H. Nishino, “Active thermographic inspection of carbon fiber reinforced plastic laminates using laser scanning heating,” *Compos. Struct.*, 2019.
- [28] W. Swiderski, “Non-destructive testing of CFRP by laser excited thermography,” *Composite Structures*. 2019.
- [29] C. Ibarra-Castanedo *et al.*, “Comparative study of active thermography techniques for the nondestructive evaluation of honeycomb structures,” *Res. Nondestruct. Eval.*, 2009.
- [30] Y. Zhao, X. Guo, M. Ren, X. Wang, and Y. He, “Lock-in thermography method for the NDT of composite materials,” 2008, vol. 7375, p. 73753V.
- [31] C. Meola, G. M. Carlomagno, A. Squillace, and A. Vitiello, “Non-destructive evaluation of aerospace materials with lock-in thermography,” *Eng. Fail. Anal.*, 2006.
- [32] L. D. Favro and X. Han, “Thermal wave material characterization and thermal wave imaging,” in *Sensing for Materials Characterization, Processing, and Manufacturing*, 1998.
- [33] G. Busse and A. Rosencwaig, “Subsurface imaging with photoacoustics,” *Appl. Phys. Lett.*, 1980.
- [34] J. C. J. H. S. Carslaw, *Conduction of Heat in Solids*, , Oxford. 1959.
- [35] A. Nanayakkara, S. Feih, and A. P. Mouritz, “Experimental analysis of the through-thickness compression properties of z-pinned sandwich composites,” *Compos. Part A Appl. Sci. Manuf.*, vol. 42, no. 11, pp. 1673–1680, 2011.
- [36] E. Ayorinde, R. Ibrahim, V. Berdichevsky, M. Jansons, and I. Grace, “Development of damage in some polymeric foam-core sandwich beams under bending loading,” *J. Sandw. Struct. Mater.*, vol. 14, no. 2, pp. 131–156, 2012.
- [37] S. Masmoudi, A. El Mahi, and R. El Guerjouma, “Mechanical behaviour and health monitoring by acoustic emission of sandwich composite integrated by piezoelectric implant,” *Compos. Part B Eng.*, 2014.
- [38] F. Pashmforoush, R. Khamedi, M. Fotouhi, M. Hajikhani, and M. Ahmadi, “Damage Classification of Sandwich Composites Using Acoustic Emission Technique and k-means Genetic Algorithm,” *J. Nondestruct. Eval.*, vol. 33, no. 4,

- pp. 481–492, 2014.
- [39] M. Fotouhi, M. Saeedifar, S. Sadeghi, M. Ahmadi Najafabadi, and G. Minak, “Investigation of the damage mechanisms for mode I delamination growth in foam core sandwich composites using acoustic emission,” *Struct. Heal. Monit.* , vol. 14, no. 3, pp. 265–280, 2015.
- [40] F. E. Oz, N. Ersoy, M. Mehdikhani, and S. V. Lomov, “Multi-instrument in-situ damage monitoring in quasi-isotropic CFRP laminates under tension,” *Compos. Struct.*, 2018.
- [41] I. E. Tabrizi, A. Kefal, J. S. M. Zanjani, C. Akalin, and M. Yildiz, “Experimental and numerical investigation on fracture behavior of glass/carbon fiber hybrid composites using acoustic emission method and refined zigzag theory,” *Compos. Struct.*, 2019.
- [42] I. E. Tabrizi *et al.*, “Determining tab material for tensile test of CFRP laminates with combined usage of digital image correlation and acoustic emission techniques,” *Compos. Part A Appl. Sci. Manuf.*, 2019.
- [43] H. Q. Ali, I. Emami Tabrizi, R. M. A. Khan, A. Tufani, and M. Yildiz, “Microscopic analysis of failure in woven carbon fabric laminates coupled with digital image correlation and acoustic emission,” *Compos. Struct.*, 2019.
- [44] A. Uzal, F. O. Sonmez, F. E. Oz, K. Cinar, and N. Ersoy, “A composite sandwich plate with a novel core design,” *Compos. Struct.*, 2018.
- [45] ASTM Standard C273, “ASTM C393-06 Standard Test Method for Core Shear Properties of Sandwich Constructions by Beam Flexure,” *ASTM Int.*, 2010.